A KINEMATIC MODEL OF CONTINUOUS SEPARATION AND CLASSIFICATION OF POLYDISPERSE SUSPENSIONS

R. BÜRGER[A], A. GARCÍA[A], K.H. KARLSEN[B], AND J.D. TOWERS[C]

Abstract. Kinematic models for polydisperse suspensions are based on specifying the solid-fluid relative velocity for each solids species as a function of the local solids concentrations. One such model, the Masliyah-Lockett-Bassoon (MLB) model, is employed herein to simulate continuous separation and classification of polydisperse suspensions. To this end, the clarifier-thickener (CT) setup for the continuous separation of suspensions is extended to a generalized clarifier-thickener (GCT). Discharge streams (or products) are described by new singular sink terms. Combining the GCT setup with the MLB model yields a system of nonlinear conservation laws with a discontinuous flux and a new nonconservative transport term describing the sinks. A numerical algorithm for the solution of this equation is presented along with numerical examples. The model describes the GCT unit with all critical design parameters, and predicts the composition of the overflow, underflow and discharge streams and the spatio-temporal evolution of the solids species concentrations inside the unit.

1. Introduction

Kinematic models are common approximate descriptions for multiphase flows that are essentially one-dimensional, for example in columns and ducts that are aligned with the driving body force. Usually, in these applications the relative (differential) movement of the phases is more important than are lateral flow components, and one continuous phase

Date: February 12, 2007.

Key words and phrases. Suspensions, sedimentation, numerical analysis, simulation, clarifier-thickeners, classification.

[A]Departamento de Ingeniería Matemática, Facultad de Ciencias Físicas y Matemáticas, Universidad de Concepción, Casilla 160-C, Concepción, Chile. E-Mail: rburger@ing-mat.udec.cl, agarcia@ing-mat.udec.cl.

[B]Centre of Mathematics for Applications (CMA), University of Oslo, P.O. Box 1053, Blindern, N–0316 Oslo, Norway. E-Mail: kennethk@math.uio.no.

[C]MiraCosta College, 3333 Manchester Avenue, Cardiff-by-the-Sea, CA 92007-1516, USA. E-mail:john.towers@cox.net.

(for solid-liquid suspensions, the fluid), and N disperse phases (species) are distinguished. We here consider polydisperse suspensions with a finite number N of solid particle species, where particles of species i have diameter d_i and density ρ_i, and $d_i \neq d_j$ or $\rho_i \neq \rho_j$ for $i \neq j$.

Kinematic models are based on the specification of the velocity of each species relative to that of the fluid as a function of the local concentrations of all species. For batch settling, this leads to a strongly coupled system of N nonlinear and spatially one-dimensional scalar conservation laws for the volume fractions $\phi_1, \ldots, \phi_N$ of all species. The extension to a continuously operated clarifier-thickener (CT) unit with a singular feed source leads to a system with an additional transport flux whose velocity is a discontinuous function of the spatial position.

We are aware of the progress has been made over the past 10 years concerning the two-and three-dimensional modelling of the flow of particles in fluidized beds, including, for example, the works of Tsuji and co-workers (Tsuji et al., 1993, 1998; Gera et al., 1998; Kawaguchi et al., 1998, 2000; Yamamoto et al., 2001) and Glowinski, Joseph, Pan and their collaborators (Glowinski et al., 2001; Pan et al., 2002) for gas-solid and liquid-solid fluidized beds, respectively. Results of fluidized bed modelling are also well documented in the monographs by Crowe et al. (1998), Jackson (2000) and Gibilaro (2001) and in the slightly older book by Gidaspow (1994); for the alternative two-phase flow and discrete particle modelling approaches, we also refer to the reviews by Enwald et al. (1996) and Deen et al. (2007). Most of the cited works are biased towards providing insight into the interaction between the fluid and individual particles, or between individual particles. They consider relatively small numbers of particles, which in turn are relatively large compared with the vessel interior diameter so that wall effects are dominant. Moreover, these models are associated with considerable computational effort. In contrast to this, our model is motivated by industrial applications, in which the particles are small with respect to the vessel diameter and computational effort in calculating each of them would be excessive. A one-dimensional description is adequate, since for small particles in liquid-solid fluidized beds, velocities and compisitions are mostly horizontal in the lateral direction. In addition, the model presented herein is supposed to form the basis of design and control calculations, for which low computational cost is desirable. This view is implicitly adapted in many engineering treatments of fluidized beds, see for example Chen et al. (2002a, b), Greenspan and Ungarish (1982), Kim and Klima (2004), Nasr-el-Din et al. (1988, 1990, 1999), Zeidan et al. (2003, 2004), and other work cited herein.

In this paper, we present a new model for continuous separation and classification of polydisperse suspensions, which extends the CT setup (Berres et al., 2004; Bürger et al., 2004; Diehl, 2006; Zeidan et al., 2004). The new feature are singular sinks describing the continuous discharge of products at several points, whose composition will vary during a transient startup procedure. The mathematical treatment and discretization of a singular sink is not entirely analogous to that of a singular feed source, since the composition of the sink stream is part of the solution. The singular sinks give rise to a novel so-called non-conservative transport term. The well-posedness of the resulting model and the convergence of a numerical scheme for $N = 1$ are proved by Bürger et al. (2006b). We herein formulate an analogous model for a generalized clarifier-thickener (GCT) setup, which may include several sinks, can also be operated as a fluidization column, and is allowed to have a varying cross-sectional area. We define a numerical scheme for its simulation and present numerical examples, in part adopting data from the literature.

The remainder of the paper is organized as follows. We briefly outline in Section 2.1 kinematic models for polydisperse suspensions, recall in Section 2.2 recent advances in the analysis and simulation of CT models, and review in Section 2.3 related work from the literature. In Section 3 we outline the kinematic model of polydisperse suspensions due to Masliyah (1979) and Lockett and Bassoon (1979) (MLB model), and recall its stability properties. In Section 4 we describe the GCT setup by balancing feed, sink, discharge and overflow bulk flows, and combine it with the MLB model to obtain the final model, which is a system of balance laws, where the nonlinear flux vector depends discontinuously on the space variable and a non-conservative transport term models the new sink feature. The numerical scheme proposed in Section 5 for the final model is based on a scheme by Kurganov and Tadmor (2000). In Section 5.1, we describe the scheme for the spatio-temporal evolution of the solids concentrations in the interior of the GCT, while Section 5.2 provides a method to calculate the sink concentrations. Section 6 presents three different numerical examples, and Section 7 collects some conclusions.

2. Motivation

2.1. **Kinematic sedimentation models.** The basic postulate of the kinematic model by Kynch (1952) states that the settling velocity v_s of a particle in a monodisperse suspension of solids concentration ϕ is given by $v_\mathrm{s} = v_\infty(1-\phi)^2 V(\phi)$, where v_∞ is the settling velocity of a

single particle in an unbounded fluid, and $V(\phi)$ is a hindered settling factor that takes into account the presence of other particles. This function can for example, be chosen as (Richardson and Zaki, 1954)

$$V(\phi) = \begin{cases} (1-\phi)^{n-2} & \text{for } \phi \in [0, \phi_{\max}], \\ 0 & \text{otherwise,} \end{cases} \qquad n > 2, \tag{2.1}$$

where $0 < \phi_{\max} \leq 1$ is a maximum concentration, and n is specified later. The one-dimensional solids continuity equation then turns into the following conservation law, where t is time and x is depth:

$$\partial_t \phi + \partial_x f(\phi) = 0, \quad f(\phi) = \phi v_{\mathrm{s}} = v_\infty \phi (1-\phi)^2 V(\phi),$$

which describes the settling of a suspension in a column. Due to the nonlinearity of $f(\phi)$, its solutions of are in general discontinuous.

For polydisperse suspensions, the sought quantity is the vector $\Phi := (\phi_1, \ldots, \phi_N)^{\mathrm{T}}$ as a function of x and t, where ϕ_i is the concentration of species i having diameter d_i and density ρ_i. For batch settling of an N-disperse suspension with initial concentration $\Phi_0(z)$ in a column of height L, the kinematic model can be expressed as the initial-boundary value problem of a system of conservation laws

$$\begin{aligned} &\partial_t \Phi + \partial_x \mathbf{f}(\Phi) = 0, \\ &\Phi(x,0) = \Phi_0(x), \ 0 \leq x \leq L; \quad \mathbf{f}|_{x=0} = \mathbf{f}|_{x=L} = 0, \quad t > 0, \end{aligned} \tag{2.2}$$

where $\mathbf{f}(\Phi) = (f_1(\Phi), \ldots, f_N(\Phi))^{\mathrm{T}}$ is the vector of flux densities $f_i(\Phi) = \phi_i v_i$, where v_i, is the velocity of particle species i, $i = 1, \ldots, N$. Choices of $\mathbf{f}(\Phi)$ proposed in the literature are compared by Ha and Liu (2002), Bürger et al. (2000, 2002) and Zeidan et al. (2003). In this paper, we adopt the MLB model (Masliyah, 1979; Lockett and Bassoon, 1979). Our preference of this model is based on the experimental study by Law et al. (1987) and analyses of global stability (Bürger et al., 2002; Berres et al., 2003). Since each function $f_i(\Phi)$ depends nonlinearly on all concentrations $\phi_1, \ldots, \phi_N$, and exact solution constructions are at least complicated (Greenspan and Ungarish, 1982; Fried and Roy, 2003), numerical methods are needed for the solution of (2.2). Clearly, its solutions are also in general discontinuous.

2.2. **Clarifier-thickener models.** The model (2.2) can be extended to continuous flow if a linear transport term $q(x,t)\Phi$ is added to the flux $\mathbf{f}(\Phi)$, which describes the differential motion of the species. The velocity $q(x,t)$ is controlled externally. We then obtain the system

$$\partial_t \Phi + \partial_x \big(q(x,t)\Phi + \mathbf{f}(\Phi) \big) = 0. \tag{2.3}$$

Models of continuously operated CT units have a clarification zone, corresponding to depth $x < 0$, adjacent to a thickening zone with $x > 0$. The feed mechanism is represented as a singular source sitting at $x = 0$. Usually, part of the feed bulk flow is directed into the thickening zone (this can be controlled by a discharge valve), while the remainder flows upwards into the clarification zone. This means that

$$q(x,t) = \begin{cases} q_{\mathrm{L}}(t) < 0 & \text{for } x < 0, \\ q_{\mathrm{R}}(t) > 0 & \text{for } x > 0, \end{cases} \tag{2.4}$$

so that the total flux $q(x,t)\Phi + \mathbf{f}(\Phi)$ is discontinuous across $x = 0$. If the unit is operated as a fluidization column, then we have $q(x,t) < 0$ throughout, but this quantity is equally discontinuous across $x = 0$. We continue to refer to "clarifier-thickener" units for polydisperse suspensions, even if in the latter case they are used for classification.

The basic difficulty is that the discontinuous flux model (2.3), (2.4) is not well posed a priori, and that numerical methods need to be tailored for its simulation. In fact, even in the scalar (monodisperse) case, the well-posedness of (2.3), (2.4) (i.e., existence and uniqueness of a properly defined solution) is not a straightforward limit case of the standard theory for conservation laws with a flux that depends smoothly on x. Even when q is constant, and $N = 1$, solutions of (2.3) are in general discontinuous, and require an entropy condition to select the physically relevant solution. In addition, they are also discontinuous across the stationary jumps of $q(x,t)$, which calls for the application of a further entropy condition. The design of entropy conditions in order to single out a unique admissible solution for a conservation law with discontinuous flux is a topic of current research. The extension of findings of mathematical analysis for $N = 1$ to $N \geq 2$ is strongly based on numerical experimentation. We refer to Zeidan et al. (2004) and Bürger et al. (2006a) for details and references.

The new ingredient of the GCT setup are one or several singular sinks, which affect the continuity equation in two ways: first, the deviation of part of the bulk flow through a sink causes a new discontinuity of $q(x,t)$, and second, the extraction of solids through a sink gives rise to an additional solution-dependent singular term. Combining both ingredients admits to replace the new flux discontinuity and the singular term by a non-conservative transport term. For $N = 1$ we poved that the model is well posed (Bürger et al., 2006a).

2.3. **Related work.** Several groups of researchers have proposed mathematical models and numerical techniques for, and conducted experiments with separation devices that are special cases of our GCT setup.

Nasr-el-Din et al. (1988, 1990, 1999) study vertical columns for the gravity separation and classification of polydisperse suspensions that have a feed source at a central depth level, and which are tapped near the top and bottom ends. They also present a mathematical model which, however, handles the steady-state case only. Experimental results for a similar setup are also presented by Spannenberg et al. (1996).

A shortcoming of the model outlined in Nasr-el-Din et al. (1988, 1990, 1999) is their source zone of finite depth, in which the composition of the mixture is supposed to be uniform and which acts as a buffer between the downwards- and upwards-directed bulk flows (if the unit is operated as the CT mode, that is, with a co-gravity bulk flow in the thickening zone), so that these flows take place in spatially separated regions. Moreover, Nasr-el-Din et al. (1999) require that "the solids and the carrier fluid are allowed to exit through the overflow or the underflow boundaries, but they are not allowed to enter the source zone through the feed stream". However, a CT model in which the clarification and thickening zones are disconnected does not capture interesting cases such as solids breaking through into the clarification zone due to overload, and it cannot be easily modified to the accommodate the fluidization column mode of operation (in which the thickening zone is fluidized by a counter-gravity bulk flow).

Chen et al. (2002a, b) develop a model of a liquid fluidized-bed classifier, first for steady state (Chen et al., 2002a) and then for the transient case (Chen et al., 2002b). (A closely related experimental study is that of Mitsutani et al. (2005).) The model is similar to ours in the fluidization column mode of operation, but differs in the detailed treatment of sources, sinks, overflows and boundary conditions. It is based on both the continuity equation and the linear momentum balance for each particle species, and includes several regularizing elements, in particular an axial dispersion (in mathematical terms, diffusion) coefficient, by which, as the authors write, "turbulence and non-uniformities are [...] taken into account indirectly". Mathematically, this term acts as a regularizing diffusion term. Moreover, the feed source and discharge sink are blended in over a finite depth interval (by means of the parameter α in Table 1 of Chen et al., 2002b), and the imposed boundary condition is equivalent to stating that the concentrations are continuous across the overflow and underflow levels. The latter condition is consistent with the global diffusion assumed by Chen et al. (2002b), but is incompatible with the condition of equality of fluxes for a kinematic model. Our approach shows that regularizing ingredients, which tend to blur features of a "true" solution such as sharp interfaces, are unnecessary, and that a complete GCT model can be based on a kinematic

approach with singular sources, sinks, and flux transitions at overflow and underflow or fluidization levels.

A similar model of a so-called hindered-settling column was proposed by Kim and Klima (2004), see also Young and Klima (2000) for experimental findings. Kim and Klima (2004) solve a scalar convection-diffusion equation for each species, which represents the continuity equation. Again, positive diffusivity is introduced, this time called a "mixing coefficient". The setup considered by Kim and Klima (2004) is that of a clarifier-thickener. One remarkable feature of the discretization chosen by Kim and Klima (2004) is that the overflow, underflow and feed mechanisms are assigned to one cell each, of the same width Δz as that of the discretization, so that their sinks and sources become singular in the limit $\Delta z \to 0$. Unfortunately, Kim and Klima (2004) do not indicate the precise algebraic treatment of these mechanisms.

The model of Zeidan et al. (2004) is equivalent to ours in the special case that there are no sinks, and a cylindrical vessel is considered. Thus, our GCT setup and its numerical treatment can be viewed as a direct extension of the model by Zeidan et al. (2004). Moreover, they use Godunov's method for discretization of the governing equations. This method is sound, but only first-order accurate, while our method is second-order accurate both in time and space. (Of course, the formal order of accuracy is recovered on smooth portions of the solution only.) The discretization chosen by Zeidan et al. (2004) is extremely coarse; the entire CT unit is subdivided into 8 cells only.

3. Mathematical model of polydisperse sedimentation

3.1. **Model equations.** Model equations for the three-dimensional motion of a polydisperse suspension were derived from the mass and linear momentum balances for the fluid and each solid species, considered as $N+1$ separate phases, by introducing constitutive assumptions and simplifying the equations through a dimensional analysis (Berres et al., 2003). The result is a particular expression of the solid-fluid relative velocity of each species as a function of Φ, which in one space dimension is equivalent to expressions stated by Masliyah (1979) and Lockett and Bassoon (1979), see (3.5) below.

We denote by $\phi := \phi_1 + \cdots + \phi_N$ the total solids concentration. If v_f is the fluid phase velocity, and $S(x)$ is the cross-sectional area of the vessel at depth x, then the one-dimensional continuity equations for the N solids phases and the fluid can be written as

$$S(x)\partial_t\phi_i + \partial_x\big(S(x)\phi_i v_i\big) = 0, \quad i = 1, \ldots, N, \tag{3.1}$$

$$-S(x)\partial_t\phi + \partial_x\big(S(x)(1-\phi)v_\mathrm{f}\big) = 0. \tag{3.2}$$

Introducing the volume average flow velocity weighted with $S(x)$,

$$Q(x,t) := S(x)\big(\phi_1 v_1 + \cdots + \phi_N v_N + (1-\phi)v_{\mathrm{f}}\big), \tag{3.3}$$

we obtain by adding (3.1) and (3.2) the mixture continuity equation $\partial_x Q(x,t) = 0$. Since a constitutive equation will be introduced for the solid-fluid relative velocities or slip velocities $u_i := v_i - v_{\mathrm{f}}$, $i = 1, \ldots, N$, we use (3.3) and $\partial_x Q(x,t) = 0$ to rewrite (3.1) as

$$\begin{aligned} &S(x)\partial_t \phi_i + \partial_x \left(Q(x,t)\phi_i + S(x)\phi_i \left[u_i - \sum_{j=1}^{N} \phi_j u_j \right] \right) = 0, \\ &i = 1, \ldots, N. \end{aligned} \tag{3.4}$$

We define the parameters $\delta_i := d_i^2/d_1^2$ and $\bar{\rho}_i := \rho_i - \rho_{\mathrm{f}}$ for $i = 1, \ldots, N$, and $\mu := g d_1^2/(18\mu_{\mathrm{f}})$, where ρ_{f} and μ_{f} are the density and the viscosity of the fluid, respectively, and g is the acceleration of gravity.

Within the MLB model, u_i is specified as

$$u_i = u_i(\Phi) = \frac{\mu\delta_i}{1 + 0.15\mathrm{Re}_i^{0.687}} V(\phi)(\bar{\rho}_i - \bar{\boldsymbol{\rho}}^{\mathrm{T}}\Phi), \quad i = 1, \ldots, N, \tag{3.5}$$

where $\bar{\boldsymbol{\rho}} := (\bar{\rho}_1, \ldots, \bar{\rho}_N)^{\mathrm{T}}$, the hindered settling factor $V(\phi)$ may be chosen as (2.1), and Re_i is the particle Reynolds number for species i,

$$\mathrm{Re}_i := |u_i|(1-\phi)\frac{d_i \rho_{\mathrm{f}}}{\mu_{\mathrm{f}}}. \tag{3.6}$$

The pair of equations (3.5) and (3.6) (see e.g. Masliyah, 1979) defines u_i implicitly. To avoid this implicit form and to be consistent with previous work, in particular, with the stability analysis of Bürger et al. (2002), we approximate Re_i by

$$\mathrm{Re}_i \approx \widetilde{\mathrm{Re}}_i := \mu\delta_i|\rho_i - \rho_{\mathrm{f}}|(1 - \beta\phi_{\max})^n \frac{d_i\rho_{\mathrm{f}}}{\mu_{\mathrm{f}}}, \tag{3.7}$$

where $\beta \in [0,1]$ is a constant parameter that has to be adjusted, and the exponent n is specified below.

For sufficiently small Reynolds numbers, namely less than 0.2, we may set the denominator in (3.5) to one. To be definite, we utilize

$$\begin{aligned} &u_i = \mu\tilde{\delta}_i V(\phi)(\bar{\rho}_i - \bar{\boldsymbol{\rho}}^{\mathrm{T}}\Phi), \\ &\tilde{\delta}_i := \begin{cases} \delta_i & \text{if } \widetilde{\mathrm{Re}}_i < 0.2, \\ \delta_i/\big(1 + 0.15\widetilde{\mathrm{Re}}_i^{0.687}\big) & \text{otherwise,} \end{cases} \quad i = 1, \ldots, N. \end{aligned} \tag{3.8}$$

The specific property of the MLB model is the appearance of the factor $V(\phi)(\bar{\rho}_i - \bar{\boldsymbol{\rho}}^{\mathrm{T}}\Phi)$ in (3.5), which in a reduced form reflects the linear momentum balances.

For spherical particles, the exponent n depends on the particle Reynolds number at infinite dilution and the particle to vessel diameter ratio, and may be given by (Richardson and Zaki, 1954)

$$n = \begin{cases} 4.65 + 19.5d/W & \text{for } \mathrm{Re}_\infty \le 0.2, \\ (4.35 + 17.5d/W)\mathrm{Re}_\infty^{-0.03} & \text{for } 0.2 < \mathrm{Re}_\infty \le 1, \\ (4.45 + 18d/W)\mathrm{Re}_\infty^{-0.1} & \text{for } 1 < \mathrm{Re}_\infty \le 200, \\ 4.45\mathrm{Re}_\infty^{-0.1} & \text{for } 200 < \mathrm{Re}_\infty \le 500, \\ 2.39 & \text{for } \mathrm{Re}_\infty > 500, \end{cases} \tag{3.9}$$

according to Richardson and Zaki (1954). Here, d is the diameter of the particles, W is the vessel diameter (of the cylindrical section of its interior), and $\mathrm{Re}_\infty := \rho_\mathrm{f} v_\infty d/\mu_\mathrm{f}$ is the particle Reynolds number based on the particle settling velocity at infinite dilution, v_∞, which we calculate as follows (Kunii and Levenspiel, 1991):

$$v_\infty = \frac{(\mu_\mathrm{f}(\rho_\mathrm{s} - \rho_\mathrm{f})g)^{1/3}}{\rho_\mathrm{f}^{2/3}\left(\dfrac{18}{(d^*)^2} + \dfrac{0.591}{(d^*)^{0.5}}\right)}, \quad d^* := d\left(\frac{\rho_\mathrm{f}(\rho_\mathrm{s} - \rho_\mathrm{f})g}{\mu_\mathrm{f}^2}\right)^{1/3}. \tag{3.10}$$

In our examples, we calculate N exponents $n_1, \ldots, n_N$ using (3.9) and (3.10) with d and ρ_s replaced by d_i and ρ_i, respectively, for $i = 1, \ldots, N$, and finally use $n = (n_1 + \cdots + n_N)/N$ in the hindered settling factor.

Inserting (3.5) into (3.4) yields the system of conservation laws

$$S(x)\partial_t \Phi + \partial_x\big(Q(x,t)\Phi + S(x)\mathbf{f}^\mathrm{M}(\Phi)\big) = 0, \tag{3.11}$$

where the components of the vector

$$\mathbf{f}^\mathrm{M}(\Phi) := \big(f_1^\mathrm{M}(\Phi), \ldots, f_N^\mathrm{M}(\Phi)\big)^\mathrm{T} \tag{3.12}$$

are the MLB flux functions $f_1^\mathrm{M}(\Phi), \ldots, f_N^\mathrm{M}(\Phi)$ given by

$$f_i^\mathrm{M}(\Phi) := \mu V(\Phi)\phi_i \left[\tilde{\delta}_i(\bar{\rho}_i - \bar{\boldsymbol{\rho}}^\mathrm{T}\Phi) - \sum_{k=1}^{N} \tilde{\delta}_k \phi_k (\bar{\rho}_k - \bar{\boldsymbol{\rho}}^\mathrm{T}\Phi)\right], \quad i = 1, \ldots, N. \tag{3.13}$$

3.2. **Stability of the MLB model.** The system (2.2) is called *hyperbolic* if the eigenvalues of the Jacobian $\mathcal{J}_\mathbf{f}(\Phi) := (\partial f_i/\partial \phi_k)_{1 \le i,k \le N}$ are real, and *strictly hyperbolic* if these are also pairwise distinct. For $N = 2$, a system with a pair of complex conjugate eigenvalues is *elliptic*. Some of the flux density vectors $\mathbf{f}(\Phi)$ proposed in the literature cause (2.2) to be of mixed type, depending on the size and density parameters, where the type is called *mixed* if the system is non-hyperbolic for certain choices of Φ.

The criterion for ellipticity is equivalent to the instability criterion by Batchelor and Janse van Rensburg (1986). Bürger et al. (2002) showed that loss of hyperbolicity, that is the occurrence of complex eigenvalues of $\mathcal{J}_{\mathbf{f}}(\Phi)$, provides an instability criterion for polydisperse suspensions for arbitrary N. For $N = 3$, this criterion can be evaluated by a convenient calculation of a discriminant, which is an explicit algebraic function of pointwise values of the partial derivatives $\partial f_i/\partial\phi_j$. Biesheuvel et al. (2001) and Bürger et al. (2002) determine instability regions for $N = 2, 3$ and different choices of $\mathbf{f}(\Phi)$. Berres et al. (2003) proved that for equal-density particles ($\bar\rho_1 = \cdots = \bar\rho_N = \rho_\mathrm{s} - \rho_\mathrm{f}$) and arbitrary particle size distributions with $\tilde\delta_i \neq \tilde\delta_j$ for $i \neq j$, the system (2.2) with the flux vector $\mathbf{f}(\Phi)$ given by (3.12), (3.13) is strictly hyperbolic for all $\Phi \in \mathcal{D}_1$ with $\phi_1 > 0, \ldots, \phi_N > 0$ and $\phi < 1$.

The instability criterion for one-dimensional batch settling is the same as for the full two- or three-dimensional model, in which the corresponding first-order system of conservation laws is coupled with additional equations of motion for the mixture. Likewise, for a given vector Φ the equation (3.11) and the final governing equation for the GCT developed herein (see Section 4.3) is instable if and only if the system (2.2) with (3.12), (3.13) is.

Biesheuvel et al. (2001) provide a vivid description of the consequences of lack of stability, which include the formation of blobs and "fingers" in bidisperse sedimentation, increased sedimentation rates, decreased separation quality of hydraulic classifiers, and non-homogeneous sediments in material manufacturing by suspension processing. These phenomena have indeed been observed in experiments (e.g. by Weiland et al., 1984) under the circumstances predicted by the instability criterion. On the other hand, the hyperbolicity, and thus stability result for equal-density spheres agrees with experimental evidence, since instabilities never have been observed with this type of mixtures, but always involve particles of different densities (Weiland et al., 1984).

For one-dimensional kinematic models, such as ours, lack of stability may lead to anomalous behaviour of the numerical solution, for example to oscillations or a "locking" effect, i.e., heavy and buoyant particles block each other within the vessel; such an example is presented by Berres et al. (2004, Figure 10). These phenomena do, however, not appear in the examples of this paper.

4. The generalized clarifier-thickener (GCT) model

We consider a vessel with axisymmetric circular interior cross-sectional area and circular cylindrical outer pipes, see Figure 1. This unit

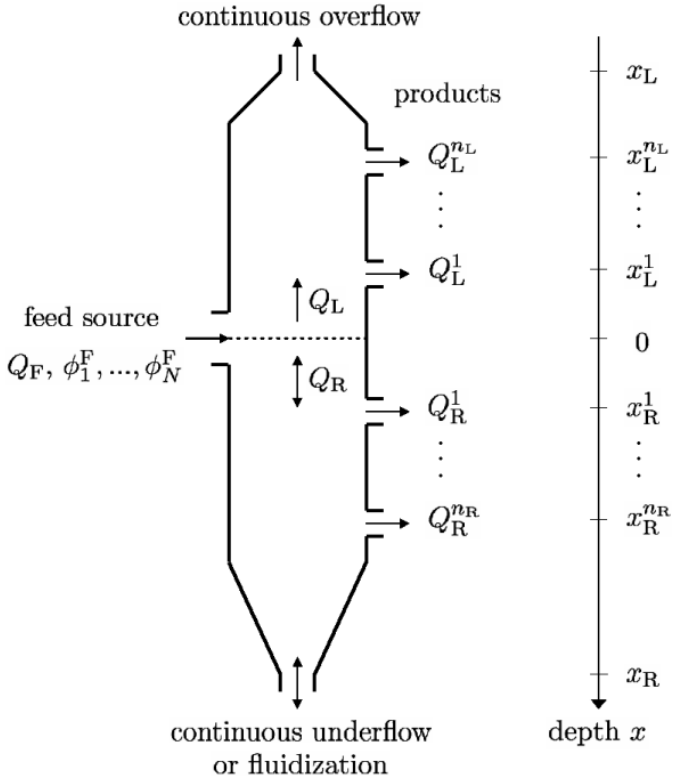

FIGURE 1. Generalized clarifier-thickener (GCT).

can be operated continuously in two modes, the clarifier-thickener (CT) mode and the fluidization column (FC) mode. In the CT mode, the feed flow is divided into upwards- and downwards-directed bulk flows, and the upper and lower ends of the unit are identified as overflow and underflow levels, respectively, whereas in the FC mode, there is an additional counter-gravity bulk inflow of liquid from $x = x_{\mathrm{R}}$. Our numerical examples are limited to the FC mode; for examples of the CT mode, we refer to Berres et al. (2004) and Bürger et al. (2006b).

We subdivide the unit into four different zones: the overflow zone ($x < x_{\mathrm{L}}$), the clarification zone ($x_{\mathrm{L}} < x < 0$), the settling zone ($0 < x < x_{\mathrm{R}}$), and the underflow (in CT mode) or fluidization (in FC mode) zone ($x > x_{\mathrm{R}}$). The vessel is continuously fed at depth $x = 0$, the feed level, with fresh feed suspension, and it has discharge outlets for products at different depths located above and below the feed point.

4.1. **Suspension bulk flows.** If $Q_{\mathrm{F}}(t) \geq 0$ is the volume feed rate of suspension, and assuming for a moment that the discharge outlets are

not active, we require that the global suspension continuity equation

$$Q_{\mathrm{F}}(t) = Q_{\mathrm{R}}(t) - Q_{\mathrm{L}}(t) \tag{4.1}$$

be always satisfied, where $Q_{\mathrm{R}}(t) > 0$ and $Q_{\mathrm{R}}(t) \leq 0$ in the CT and FC modes, respectively, and $Q_{\mathrm{L}}(t) \leq 0$.

Now let us include discharge openings located at $0 > x_{\mathrm{L}}^1 > \cdots > x_{\mathrm{L}}^{n_{\mathrm{L}}} > x_{\mathrm{L}}$ and $0 < x_{\mathrm{R}}^1 < \cdots < x_{\mathrm{R}}^{n_{\mathrm{R}}} < x_{\mathrm{R}}$ associated with the respective discharge rates $Q_{\mathrm{L}}^1(t) \leq 0, \ldots, Q_{\mathrm{L}}^{n_{\mathrm{L}}}(t) \leq 0$ and $Q_{\mathrm{R}}^1(t) \leq 0, \ldots, Q_{\mathrm{R}}^{n_{\mathrm{R}}}(t) \leq 0$. We now denote by $Q_{\mathrm{L}}(t)$ and $Q_{\mathrm{R}}(t)$ the volume bulk flows adjacent to $x = 0$, so that (4.1) remains valid. Using the Heaviside function

$$H(\xi) := \begin{cases} 1 & \text{if } \xi \geq 0, \\ 0 & \text{if } \xi < 0, \end{cases}$$

we can write the piecewise constant (with respect to x) bulk flow as

$$Q(x,t) = \begin{cases} Q_{\mathrm{L}}(t) - \displaystyle\sum_{m=1}^{n_{\mathrm{L}}} Q_{\mathrm{L}}^m(t) H(x_{\mathrm{L}}^m - x) & \text{for } x < 0, \\ Q_{\mathrm{R}}(t) + \displaystyle\sum_{m=1}^{n_{\mathrm{R}}} Q_{\mathrm{R}}^m(t) H(x - x_{\mathrm{R}}^m) & \text{for } x > 0. \end{cases} \tag{4.2}$$

4.2. **Solids feed and sink terms.** As in Bürger et al. (2006a), we assume that for $x > x_{\mathrm{R}}$ and $x < x_{\mathrm{L}}$, the cross-sectional area shrinks to a very small value, so that these zones actually correspond to transport pipes in which all solids (if any) move with the velocity of the fluid. Consequently, the slip velocities $u_1, \ldots, u_N$ are "switched off" outside the vessel interior $(x_{\mathrm{L}}, x_{\mathrm{R}})$ by the discontinuous function

$$\gamma^1(x) := \begin{cases} S(x) & \text{if } x_{\mathrm{L}} < x < x_{\mathrm{R}}, \\ 0 & \text{otherwise.} \end{cases}$$

The next step is to replace (3.11) by the equation

$$S(x)\partial_t \Phi + \partial_x\big(Q(x,t)\Phi + \gamma^1(x)\mathbf{f}^{\mathrm{M}}(\Phi)\big) = 0, \tag{4.3}$$

where $Q(x,t)$ is given by (4.2). Next, we consider that at $x = 0$, the unit is fed at a volume rate $Q_{\mathrm{F}}(t) \geq 0$ with feed suspension that contains solids of species 1 to N at the volume fractions $\phi_1^{\mathrm{F}}(t)$ to $\phi_N^{\mathrm{F}}(t)$. Specifying the phase space of physically relevant concentrations

$$\mathcal{D}_{\phi_{\max}} := \big\{(\phi_1, \ldots, \phi_N)^{\mathrm{T}} : \phi_1 \geq 0, \ldots, \phi_N \geq 0,\, \phi \leq \phi_{\max}\big\},$$

where $\phi_{\max}$ is the maximal solids concentration, we assume that

$$\Phi^{\mathrm{F}}(t) := (\phi_1^{\mathrm{F}}(t), \ldots, \phi_N^{\mathrm{F}}(t))^{\mathrm{T}} \in \mathcal{D}_{\phi_{\max}} \quad \text{for all } t > 0.$$

The feed mechanism gives rise to an additional singular source term to (4.3), so that we now consider the equation

$$S(x)\partial_t\Phi + \partial_x\big(Q(x,t)\Phi + \gamma^1(x)\mathbf{f}^{\mathrm{M}}(\Phi)\big) = \delta(x)Q_{\mathrm{F}}(t)\Phi^{\mathrm{F}}(t), \tag{4.4}$$

where $\delta(x)$ is the Dirac delta function centered at $x = 0$. Using the Heaviside function and $Q_{\mathrm{R}}(t)$ and $Q_{\mathrm{L}}(t)$ as control variables, we may absorb the right-hand side of (4.4) into the flux function. Furthermore, we take into account that the *sink* terms model the discharge of suspension of *unknown* concentration. This leads to the equation

$$\begin{aligned} &S(x)\partial_t\Phi + \partial_x\Big(Q(x,t)\Phi + \gamma^1(x)\mathbf{f}^{\mathrm{M}}(\Phi) - H(x)\big(Q_{\mathrm{R}}(t) - Q_{\mathrm{L}}(t)\big)\Phi^{\mathrm{F}}(t)\Big) \\ &= \sum_{m=1}^{n_{\mathrm{L}}} \delta(x - x_{\mathrm{L}}^m)Q_{\mathrm{L}}^m(t)\Phi(x,t) + \sum_{l=1}^{n_{\mathrm{R}}} \delta(x - x_{\mathrm{R}}^l)Q_{\mathrm{R}}^l(t)\Phi(x,t), \end{aligned}$$

which can be rewritten as

$$\begin{aligned} S(x)\partial_t\Phi + \partial_x\Big(&Q(x,t)\Phi + \gamma^1(x)\mathbf{f}^{\mathrm{M}}(\Phi) + \mathcal{H}(x,t)\Phi \\ &- H(x)\big(Q_{\mathrm{R}}(t) - Q_{\mathrm{L}}(t)\big)\Phi^{\mathrm{F}}(t)\Big) = \mathcal{H}(x,t)\partial_x\Phi(x,t), \end{aligned} \tag{4.5}$$

where we define the piecewise constant (with respect to x) function

$$\mathcal{H}(x,t) := -\sum_{m=1}^{n_{\mathrm{L}}} H(x - x_{\mathrm{L}}^m)Q_{\mathrm{L}}^m(t) - \sum_{l=1}^{n_{\mathrm{R}}} H(x - x_{\mathrm{R}}^l)Q_{\mathrm{R}}^l(t).$$

4.3. **Final form of the mathematical model.** We assume that the control variables $Q_{\mathrm{F}}(t)$, $Q_{\mathrm{R}}(t)$ and $Q_{\mathrm{L}}(t)$ as well as the discharge fluxes controlling the sink terms are constant. Then, in view of (4.2), and defining $\tilde{Q}_{\mathrm{L}} := Q_{\mathrm{L}} - (Q_{\mathrm{L}}^1 + \cdots + Q_{\mathrm{L}}^{n_{\mathrm{L}}})$, we can rewrite (4.5) as

$$S(x)\partial_t\Phi + \partial_x\tilde{\mathbf{g}}(x,\Phi) = \mathcal{H}(x)\partial_x\Phi,$$

where we define

$$\tilde{\mathbf{g}}(x,\Phi) := \begin{cases} \tilde{Q}_{\mathrm{L}}\Phi + \gamma^1(x)\mathbf{f}^{\mathrm{M}}(\Phi) & \text{for } x < 0, \\ Q_{\mathrm{R}}\Phi - (Q_{\mathrm{R}} - Q_{\mathrm{L}})\Phi^{\mathrm{F}} & \\ \quad +(\tilde{Q}_{\mathrm{L}} - Q_{\mathrm{L}})\Phi + \gamma^1(x)\mathbf{f}^{\mathrm{M}}(\Phi) & \text{for } x \geq 0, \end{cases}$$

and $\mathcal{H}(x)$ is the time-independent version of $\mathcal{H}(x,t)$. Adding the constant vector $-\tilde{Q}_{\mathrm{L}}\Phi^{\mathrm{F}}$ to $\tilde{\mathbf{g}}(x,\Phi)$, and defining $\tilde{Q}_{\mathrm{R}} := Q_{\mathrm{R}} - (Q_{\mathrm{L}}^1 + \cdots + Q_{\mathrm{L}}^{n_{\mathrm{L}}})$, we obtain the flux vector

$$\mathbf{g}(x,\Phi) := \begin{cases} \tilde{Q}_{\mathrm{L}}(\Phi - \Phi^{\mathrm{F}}) + \gamma^1(x)\mathbf{f}^{\mathrm{M}}(\Phi) & \text{for } x < 0, \\ \tilde{Q}_{\mathrm{R}}(\Phi - \Phi^{\mathrm{F}}) + \gamma^1(x)\mathbf{f}^{\mathrm{M}}(\Phi) & \text{for } x \geq 0. \end{cases}$$

Defining the discontinuous parameter

$$\gamma^2(x) := \begin{cases} \tilde{Q}_{\mathrm{L}} & \text{for } x < 0, \\ \tilde{Q}_{\mathrm{R}} & \text{for } x \geq 0 \end{cases}$$

and the vector $\boldsymbol{\gamma}(x) := (\gamma^1(x), \gamma^2(x))$, we obtain

$$\mathbf{g}(x, \Phi) = \mathbf{f}\big(\boldsymbol{\gamma}(x), \Phi\big) := \gamma^1(x)\mathbf{f}^{\mathrm{M}}(\Phi) + \gamma^2(x)(\Phi - \Phi^{\mathrm{F}}).$$

This yields the governing equation

$$S(x)\partial_t \Phi + \partial_x \mathbf{f}\big(\boldsymbol{\gamma}(x), \Phi\big) = \mathcal{H}(x)\partial_x \Phi. \tag{4.6}$$

This system is solved together with the initial condition

$$\Phi(x, 0) = \Phi^0(x) := \big(\phi_1^0(x), \dots, \phi_N^0(x)\big)^{\mathrm{T}} \in \mathcal{D}_{\phi_{\max}}. \tag{4.7}$$

Note that the decisive new feature of (4.6) is the non-conservative transport term $\mathcal{H}(x)\partial_x\Phi$, which models the singular sinks.

5. Numerical scheme

5.1. **Discretization of the interior of the GCT.** We discretize the spatial domain into cells $I_j := [x_{j-1/2}, x_{j+1/2})$, $j = 0, \pm 1, \pm 2, \dots$, where $x_k = k\Delta x$ for $k = 0, \pm 1/2, \pm 1, \pm 3/2, \dots$. Similarly, the time interval $(0, T)$ is discretized via $t_n = n\Delta t$ for $n = 0, \dots, \mathcal{N}$, where $\mathcal{N} = \lfloor T/\Delta t \rfloor + 1$, which results in the time strips $I^n := [t_n, t_{n+1})$, $n = 0, \dots, \mathcal{N} - 1$. Here $\Delta x > 0$ and $\Delta t > 0$ denote the spatial and temporal discretization parameters, respectively. These parameters are chosen so that the following stability condition (CFL condition) holds:

$$\frac{\Delta t}{\Delta x S_{\min}} \Big(\max \rho\big(J_{\mathbf{f}}(\boldsymbol{\gamma}, \Phi)\big) + \max_{x \in (-\infty, \infty)} \mathcal{H}(x) \Big) \leq \frac{1}{8},$$

where $\rho(\cdot)$ denotes the spectral radius, $J_{\mathbf{f}}(\boldsymbol{\gamma}, \Phi)$ the $N \times N$ Jacobian of $\mathbf{f}(\boldsymbol{\gamma}, \Phi)$, and $S_{\min} = \min_{x \in (-\infty, \infty)} S(x)$.

In the numerical scheme, we approximate $\max \rho(J_{\mathbf{f}}(\boldsymbol{\gamma}, \Phi))$ by

$$\alpha := \max_{x \in (-\infty, \infty)} |\gamma^2(x)| + S_{\max} \max_{1 \leq i \leq N} \big\{ |v_\infty^i| \big\},$$

where $S_{\max} = \max_{x \in (-\infty, \infty)} S(x)$, and v_∞^i is given by (3.10) with d and ρ_{s} replaced by d_i and ρ_i, respectively.

Our scheme is a direct modification of the one described by Kurganov and Tadmor (2000). Let $\mathbf{U}_j^n := (U_{1,j}^n, \dots, U_{N,j}^n)^{\mathrm{T}}$ denote our approximation to $\Phi(x_j, t_n)$. Expressed in terms of the forward Euler solver,

we consider the one-parameter family of Runge-Kutta schemes

$$
\begin{aligned}
\mathbf{U}_j^{(1)} &= \mathbf{U}_j^n - \lambda_j \Delta_- \mathbf{h}\big(\boldsymbol{\gamma}_{j+1/2}, \mathbf{U}_{j-1}^n, \ldots, \mathbf{U}_{j+2}^n\big) + \lambda_j \mathcal{H}_j \, \Delta_+ \mathbf{U}_j^n, \\
\mathbf{U}_j^{(k+1)} &= (1-\eta_k)\big(\mathbf{U}_j^{(k)} - \lambda_j \Delta_- \mathbf{h}\big(\boldsymbol{\gamma}_{j+1/2}, \mathbf{U}_{j-1}^{(k)}, \ldots, \mathbf{U}_{j+2}^{(k)}\big) \\
&\qquad + \lambda_j \mathcal{H}_j \, \Delta_+ \mathbf{U}_j^{(k)}\big) + \eta_k \mathbf{U}_j^n, \qquad k = 1, 2, \ldots, s-1, \\
\mathbf{U}_j^{n+1} &:= \mathbf{U}_j^{(s)},
\end{aligned}
\tag{5.1}
$$

where we denote by $G(x^-)$ the limit of a function $G(\xi)$ for $\xi \to x$, $\xi < x$, introduce the difference operators $\Delta_- V_j := V_j - V_{j-1}$ and $\Delta_+ V_j := V_{j+1} - V_j$, and define $\boldsymbol{\gamma}_{j+1/2} := \boldsymbol{\gamma}(x_{j+1/2}^-)$, $\lambda_j := \Delta t/(S_j \Delta x)$ with $S_j := S(x_j^-)$, $\mathcal{H}_j := \mathcal{H}(x_j^-)$, and $\mathbf{U}_j^0 := \Phi_0(x_j^-)$. We employ second-order time differencing ($s = 2$), for which $\eta_1 = 1/2$; for third-order time differencing ($s = 3$), the appropriate values are $\eta_1 = 3/4$ and $\eta_2 = 1/3$.

Before describing the computation of the numerical flux vector $\mathbf{h}$, we briefly justify the scheme. The main differences between (5.1) and the scheme originally defined by Kurganov and Tadmor (2000) (KT scheme) and adapted to the CT setup by Berres et al. (2004) are the coefficient λ_j and the term $\lambda_j \mathcal{H}_j \, \Delta_+ \mathbf{U}_j^n$. The original KT scheme is a high-resolution central difference scheme for the approximation of first-order systems of conservation laws with a flux that depends continuously on Φ, such as our system (2.2). High-resolution schemes approximate smooth parts of solutions with at least second order of accuracy, and resolve discontinuities sharply and without spurious oscillations. The main advantage of the KT scheme for our model is that as a central scheme, and unlike upwind schemes, it avoids approximate Riemann solvers, projections along characteristic directions, and splittings of the flux vector in upwind and downwind directions. It shares these properties with the previous central scheme due to Nessyahu and Tadmor (1990) (NT scheme), but the KT scheme has a smaller numerical viscosity than the NT scheme, is better suited for near-steady-state solutions, and admits a convergent semi-discrete variant. Berres et al. (2004) applied this scheme to a CT model for polydisperse suspensions, compared it with alternative discretizations and demonstrated that these advantages persist when the scheme is applied to a system of conservation laws with discontinuous flux.

The new ingredient is the term $\lambda_j \mathcal{H}_j \, \Delta_+ \mathbf{U}_j^n$ that has been added to incorporate the sink feature of the model, and which discretizes the transport term $\mathcal{H}(x)\partial_x \Phi$ in the right-hand side of (4.6). Since this term is non-conservative, its discretization cannot simply be made part of the KT scheme. For the scalar case, several possibilities to discretize this term are compared by Bürger et al. (2006b); the simplest one is the

difference $\lambda_j \mathcal{H}_j \ \Delta_+ \mathbf{U}_j^n$ that has been chosen here. The orientation of the stencil is deliberate; in view of $\mathcal{H}(x) \geq 0$, we chose here the forward difference Δ_+ as a discretization that has an upwind property. Moreover, this is the discretization to which the convergence analysis for the scalar scheme introduced by Bürger et al. (2006b) directly applies.

The numerical flux vector $\mathbf{h}$ appearing in (5.1) is given by

$$\begin{aligned}&\mathbf{h}\big(\boldsymbol{\gamma}_{j+1/2}, \mathbf{U}_{j-1}^n, \ldots, \mathbf{U}_{j+2}^n\big)\\ &:= \frac{1}{2}\big[\mathbf{f}\big(\boldsymbol{\gamma}_{j+1/2}, \mathbf{U}_{j+1/2}^+(t_n)\big) + \mathbf{f}\big(\boldsymbol{\gamma}_{j+1/2}, \mathbf{U}_{j+1/2}^-(t_n)\big)\big]\\ &\quad - \frac{1}{2} a_{j+1/2}^n \big[\mathbf{U}_{j+1/2}^+(t_n) - \mathbf{U}_{j+1/2}^-(t_n)\big],\end{aligned}$$

which is expressed in terms of the intermediate values

$$\mathbf{U}_{j+1/2}^+(t_n) := \mathbf{U}_{j+1}^n - \frac{\Delta x}{2}(\Phi_x)_{j+1}^n, \quad \mathbf{U}_{j+1/2}^-(t_n) := \mathbf{U}_j^n + \frac{\Delta x}{2}(\Phi_x)_j^n,$$

and the local speeds of propagation $a_{j+1/2}^n$, which we estimate by

$$a_{j+1/2} = \gamma^1\big(x_{j+1/2}^-\big) \max\big\{|v_\infty^1|, \ldots, |v_\infty^N|\big\} + \big|\gamma^2\big(x_{j+1/2}^-\big)\big|.$$

The numerical derivatives are determined by

$$(\Phi_x)_j^n := \frac{1}{\Delta x} \mathrm{MM}\left\{\theta(\mathbf{U}_j^n - \mathbf{U}_{j-1}^n), \frac{1}{2}(\mathbf{U}_{j+1}^n - \mathbf{U}_{j-1}^n), \theta(\mathbf{U}_{j+1}^n - \mathbf{U}_j^n)\right\},$$

where $\theta \in [1, 2]$ is a parameter and $\mathrm{MM}(\cdot, \cdot, \cdot)$ is the minmod function:

$$\mathrm{MM}(a, b, c) := \begin{cases} \min\{a, b, c\} & \text{if } a, b, c > 0,\\ \max\{a, b, c\} & \text{if } a, b, c < 0,\\ 0 & \text{otherwise.}\end{cases}$$

As stated by Kurganov and Tadmor (2000), in the scalar case ($N = 1$) the value $\theta = 2$ corresponds to the least dissipative limiter, while $\theta = 1$ ensures the non-oscillatory nature of the approximate solution. The best choice of θ depends on the model considered. For systems, the optimal values of θ vary between 1.1 and 1.5 (Kurganov and Tadmor, 2000). As a compromise, and following previous works (Berres et al., 2004; Qian et al., 2005), we choose $\theta = 1.3$ in all examples.

5.2. **Calculation of the sink concentrations.** The concentrations of each species in the GCT sinks can be computed a posteriori from the concentration distribution in the interior, for example after every time interval whose length is a fixed multiple of Δt.

For a GCT with exactly one sink, the sink concentrations follow from the overall mass balance of each particle species. To specify this balance, let $\tilde{x}_\mathrm{L} := M_\mathrm{L}\Delta x$ and $\tilde{x}_\mathrm{R} := M_\mathrm{R}\Delta x$ be chosen such that $\tilde{x}_\mathrm{L} < x_\mathrm{L}$

and $\tilde{x}_{\mathrm{R}} > x_{\mathrm{R}}$, and assume that the approximate solution of the problem between these two positions has been stored. The difference between the total flow rate into and out of the vessel for particle species i must equal the accumulation rate of that particle species in it, i.e.

$$\begin{aligned} &Q(\tilde{x}_{\mathrm{L}},t)\phi_i(\tilde{x}_{\mathrm{L}},t) + Q_{\mathrm{F}}(t)\phi_i^{\mathrm{F}}(t) + Q_{\mathrm{S}}(t)\phi_i^{\mathrm{S}}(t) - Q(\tilde{x}_{\mathrm{R}},t)\phi_i(\tilde{x}_{\mathrm{R}},t) \\ &= \frac{d}{dt}\int_{\tilde{x}_{\mathrm{L}}}^{\tilde{x}_{\mathrm{R}}} \phi_i(\xi,t)S(\xi)\,d\xi, \end{aligned} \tag{5.2}$$

where $Q_{\mathrm{S}}(t)$ and $\phi_i^{\mathrm{S}}(t)$ are the volume flow rate and the volume fraction of the species i in the sink located at $x = x_{\mathrm{S}}$ at time t, respectively.

For $t = t_n$, we approximate the right-hand side of (5.2) by

$$\begin{aligned} &I_i(\tilde{x}_{\mathrm{L}},\tilde{x}_{\mathrm{R}},t_n) \\ &:= \sum_{k=M_{\mathrm{L}}+1}^{M_{\mathrm{R}}-1} \frac{U_{i,k}^{n+1}-U_{i,k}^n}{\lambda_k} + \frac{U_{i,M_{\mathrm{L}}}^{n+1}-U_{i,M_{\mathrm{L}}}^n}{2\lambda_{M_{\mathrm{L}}}} + \frac{U_{i,M_{\mathrm{R}}}^{n+1}-U_{i,M_{\mathrm{R}}}^n}{2\lambda_{M_{\mathrm{R}}}}. \end{aligned} \tag{5.3}$$

We approximate $\phi_i^{\mathrm{S}}(t_n)$ by the following formula, which follows from replacing the right-hand side of (5.2) by (5.3), and the exact solution ϕ_i by the approximate solution $U_{i,k}^n$:

$$\begin{aligned} \phi_i^{\mathrm{S}}(t_n) \approx \frac{1}{Q_{\mathrm{S}}(t_n)}\big(&I_i(\tilde{x}_{\mathrm{L}},\tilde{x}_{\mathrm{R}},t_n) - Q(\tilde{x}_{\mathrm{L}},t_n)U_{i,M_{\mathrm{L}}}^n \\ &- Q_{\mathrm{F}}(t_n)\phi_i^{\mathrm{F}}(t_n) + Q(\tilde{x}_{\mathrm{R}},t_n)U_{i,M_{\mathrm{R}}}^n\big). \end{aligned}$$

Now we consider a GCT with two or more sinks. First we explain the method for calculating the concentrations of the sinks located from x_{L}^1 to $x_{\mathrm{L}}^{n_{\mathrm{L}}}$, i.e. above the feed level. For a sink located at x_{L}^{μ}, we solve in the order $\mu = n_{\mathrm{L}}, n_{\mathrm{L}}-1, \ldots, 1$, with our numerical scheme, a set of auxiliary problems with the initial condition $\tilde{\Phi}(x,0) = \Phi(x,t_n)$. These auxiliary problems are based on the original problem (4.6), (4.7), but we turn off the sinks located at x_{L}^{μ} to $x_{\mathrm{L}}^{n_{\mathrm{L}}}$ and add their discharge rates to the bulk flow $Q(x,t)$ in $x < x_{\mathrm{L}}^{\mu}$. Then, for each t_n we write the overall mass balances of each particle species for the original problem and for the corresponding auxiliary problem. Due to the finite speed of propagation and the smallness of the time interval $[t_n, t_{n+1})$, we may assume that the concentrations of the sinks located below x_{L}^{μ} and of the underflow are the same for both problems. Then, the difference

between both mass balances of each particle species gives

$$\begin{aligned} &Q(\tilde{x}_{\mathrm{L}},t)\big(\phi_i(\tilde{x}_{\mathrm{L}},t)-\tilde{\phi}_i(\tilde{x}_{\mathrm{L}},t-t_n)\big)\\ &+\sum_{j=\mu}^{n_{\mathrm{L}}} Q_{\mathrm{L}}^j(t)\big(\phi_{i,\mathrm{L}}^j(t)-\tilde{\phi}_i(\tilde{x}_{\mathrm{L}},t-t_n)\big)\\ &=\frac{d}{dt}\int_{\tilde{x}_{\mathrm{L}}}^{\tilde{x}_{\mathrm{R}}}\big(\phi_i(\xi,t)-\tilde{\phi}_i(\xi,t-t_n)\big)S(\xi)d\xi, \end{aligned} \tag{5.4}$$

where $\tilde{\phi}_i(x,t-t_n)$ is the volume fraction of species i for the auxiliary problem, and $\tilde{\phi}_{i,\mathrm{L}}^j(t)$ is the volume fraction of species i in the sink located in x_{L}^j, $j=\mu,\dots,n_{\mathrm{L}}$, at time t. As in the case with one sink, we denote the numerical approximation of the right hand side of (5.4) as $I_{i,\mathrm{L}}^{\mu}(\tilde{x}_{\mathrm{L}},\tilde{x}_{\mathrm{R}},t)$ and replace the exact solutions ϕ_i and $\tilde{\phi}_i$ by the approximate solutions $U_{i,k}^n$ and $\tilde{U}_{i,k}^n$, respectively. Then we obtain

$$\begin{aligned} \phi_{i,\mathrm{L}}^{\mu}(t_n)\approx \tilde{U}_{i,M_{\mathrm{L}}}^n+\frac{1}{Q_{\mathrm{L}}^{\mu}(t_n)}\Bigg\{ & I_{i,\mathrm{L}}^{\mu}(\tilde{x}_{\mathrm{L}},\tilde{x}_{\mathrm{R}},t_n)-Q(\tilde{x}_{\mathrm{L}},t_n)\big(U_{i,M_{\mathrm{L}}}^n-\tilde{U}_{i,M_{\mathrm{L}}}^n\big)\\ &-\sum_{j=\mu+1}^{n_{\mathrm{L}}} Q_{\mathrm{L}}^j(t_n)\big(\phi_i^j(t_n)-\tilde{U}_{i,M_{\mathrm{L}}}^n\big)\Bigg\}. \end{aligned}$$

Note that the initial condition of the auxiliary problems implies that $U_{i,k}^n=\tilde{U}_{i,k}^n$. The value of $I_{i,\mathrm{L}}^{\mu}(\tilde{x}_{\mathrm{L}},\tilde{x}_{\mathrm{R}},t_n)$ is then calculated by

$$\begin{aligned} &I_{i,\mathrm{L}}^{\mu}(\tilde{x}_{\mathrm{L}},\tilde{x}_{\mathrm{R}},t_n)\\ &:=\sum_{k=M_{\mathrm{L}}+1}^{M_{\mathrm{R}}-1}\frac{U_{i,k}^{n+1}-\tilde{U}_{i,k}^{n+1}}{\lambda_k}+\frac{U_{i,M_{\mathrm{L}}}^{n+1}-\tilde{U}_{i,M_{\mathrm{L}}}^{n+1}}{2\lambda_{M_{\mathrm{L}}}}+\frac{U_{i,M_{\mathrm{R}}}^{n+1}-\tilde{U}_{i,M_{\mathrm{R}}}^{n+1}}{2\lambda_{M_{\mathrm{R}}}}. \end{aligned}$$

For the sinks located at x_{R}^2 to $x_{\mathrm{R}}^{n_{\mathrm{R}}}$ we follow the same method as for those located at x_{L}^1 to $x_{\mathrm{L}}^{n_{\mathrm{L}}}$. For the sink at x_{R}^1 we only use the overall mass balance of each particle species. Then we have

$$\begin{aligned} &\phi_{i,\mathrm{R}}^1(t_n)\\ &\approx\frac{1}{Q_{\mathrm{R}}^1(t_n)}\Bigg\{ I_{i,\mathrm{R}}^1(\tilde{x}_{\mathrm{L}},\tilde{x}_{\mathrm{R}},t_n)-Q(\tilde{x}_{\mathrm{L}},t_n)U_{i,M_{\mathrm{L}}}^n-Q_{\mathrm{F}}(t_n)\phi_i^{\mathrm{F}}(t_n)\\ &\quad+Q(\tilde{x}_{\mathrm{R}},t_n)U_{i,M_{\mathrm{R}}}^n-\sum_{j=1}^{n_{\mathrm{L}}}Q_{\mathrm{L}}^j(t_n)\phi_{i,\mathrm{L}}^j(t_n)-\sum_{j=2}^{n_{\mathrm{R}}}Q_{\mathrm{R}}^j(t_n)\phi_{i,\mathrm{R}}^j(t_n)\Bigg\}, \end{aligned}$$

where $I_{i,\mathrm{R}}^1(\tilde{x}_{\mathrm{L}},\tilde{x}_{\mathrm{R}},t_n)$ is calculated by (5.3).

	Example 1	Example 2	Example 3
N	3	2	6
d_1 [m]	1.5×10^{-4}	9.0×10^{-4}	2.3×10^{-3}
d_2 [m]	5.0×10^{-5}	5.5×10^{-5}	1.7×10^{-3}
d_3 [m]	3.5×10^{-5}	—	1.2×10^{-3}
d_4 [m]	—	—	8.6×10^{-4}
d_5 [m]	—	—	6.1×10^{-4}
d_6 [m]	—	—	4.0×10^{-4}
δ_2	0.1111	0.3735	0.5463
δ_3	0.0544	—	0.2722
δ_4	—	—	0.1398
δ_5	—	—	0.0703
δ_6	—	—	0.0302
ρ_1 [kg/m^3]	1050	2470*	2470*
ρ_2 [kg/m^3]	2403	—	—
ρ_3 [kg/m^3]	2850	—	—
n	4.66	2.91	2.74
ϕ_1^{F}	0.0728	0.0676	0.00787
ϕ_2^{F}	0.0676	0.0624	0.02616
ϕ_3^{F}	0.0624	—	0.03485
ϕ_4^{F}	—	—	0.02484
ϕ_5^{F}	—	—	0.01480
ϕ_6^{F}	—	—	0.01147
Q_{F} [m^3/s]	1.78×10^{-5}	5.9596×10^{-3}	6.074×10^{-3}
Q_{R} [m^3/s]	2.1×10^{-6}	-1.444×10^{-3}	-1.378×10^{-3}
Q_{L}^1 [m^3/s]	-4.2×10^{-6}	0	0
Q_{L} [m^3/s]	-1.99×10^{-5}	-7.404×10^{-3}	-7.452×10^{-3}
Q_{R}^1 [m^3/s]	-3.5×10^{-6}	-3.668×10^{-4}	-4.183×10^{-4}
Δx [10^{-3} m]	8.081	5.206	5.693
Δt [10^{-3} s]	105.0	0.1096	0.05315

TABLE 1. Parameters for the numerical simulations. $\star$: species of equal density.

6. Numerical examples

6.1. **Preliminary remarks.** We consider three GCT vessels, which are operated in FC mode and have varying cross-sectional area, see Figures 2, 7 and 12. Associated to Vessels 1, 2, and 3 are Examples 1, 2, and 3, respectively, whose parameters are given in Table 1. In all

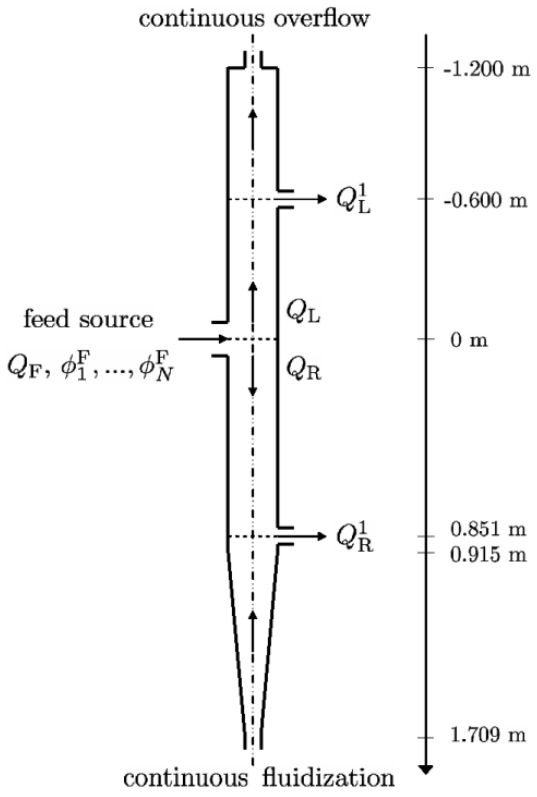

FIGURE 2. Vessel 1 with varying interior area and two sinks.

cases, the fluid is water at 20 °C with $\rho_{\mathrm{f}} = 998.2\,\mathrm{kg/m^3}$ and $\mu_{\mathrm{f}} = 1.005 \times 10^{-3}\,\mathrm{Pa\ s}$

Example 1 is "virtual" and has been included to study the behaviour of particles differing both in size and density, while Examples 2 and 3 are based on, and in part compared with, experimental data by Chen et al. (2002a) for equal-density particles. Published data on classifier-type experiments with particles having different densities is scarce; for comparisons of experiments with such suspensions with numerical simulations in the (simpler) cases of batch settling and a CT setup (without sinks), we refer to Bürger et al. (2000) and Berres et al. (2004).

To ensure that the solution assumes values in $\mathcal{D}_{\phi_{\max}}$, we replace (2.1) by the following function, which continuously goes to zero as $\phi \to \phi_{\max}$

(a)

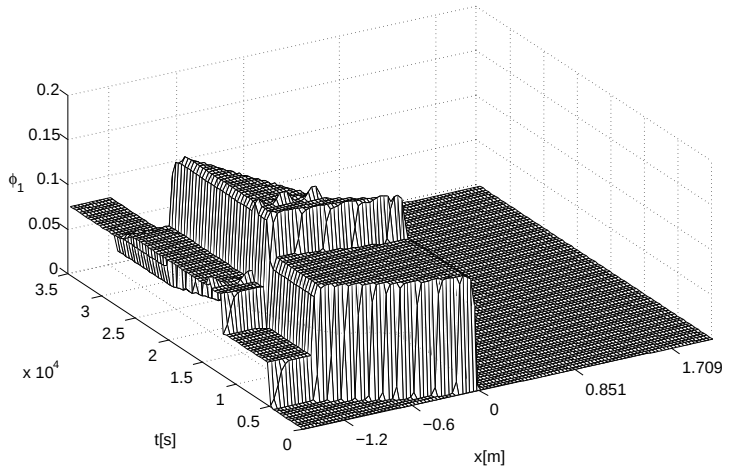

(b)

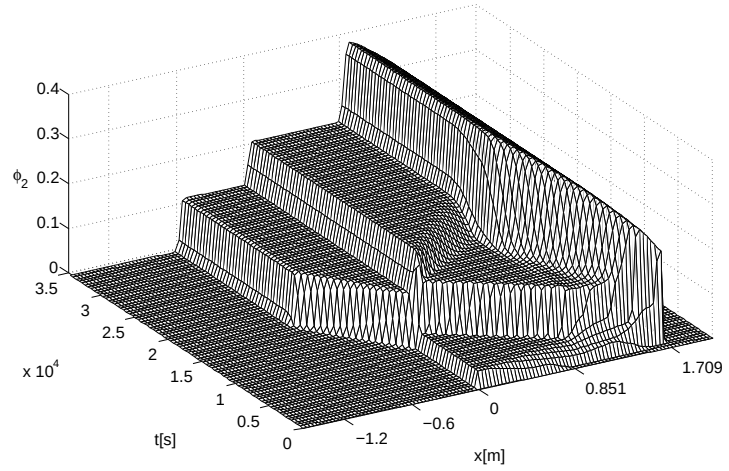

FIGURE 3. Example 1: Simulated concentrations (a) ϕ_1 (species 1), (b) ϕ_2 (species 2).

and where $0 < \phi_{\mathrm{q}} < \phi_{\max}$ is a parameter:

$$V(\phi) = \begin{cases} (1-\phi)^{n-2} & \text{for } \phi \in [0, \phi_{\mathrm{q}}), \\ (1-\phi_{\mathrm{q}})^{n-2} \dfrac{\phi_{\max} - \phi}{\phi_{\max} - \phi_{\mathrm{q}}} & \text{for } \phi \in [\phi_{\mathrm{q}}, \phi_{\max}], \quad n > 2. \\ 0 & \text{otherwise,} \end{cases} \tag{6.1}$$

(a)

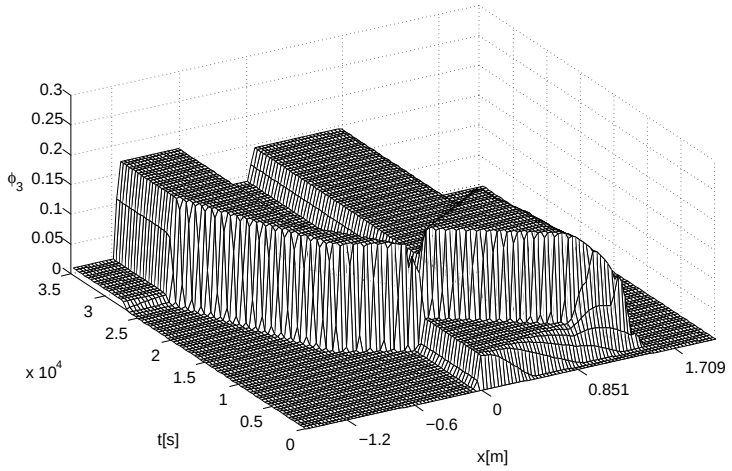

(b)

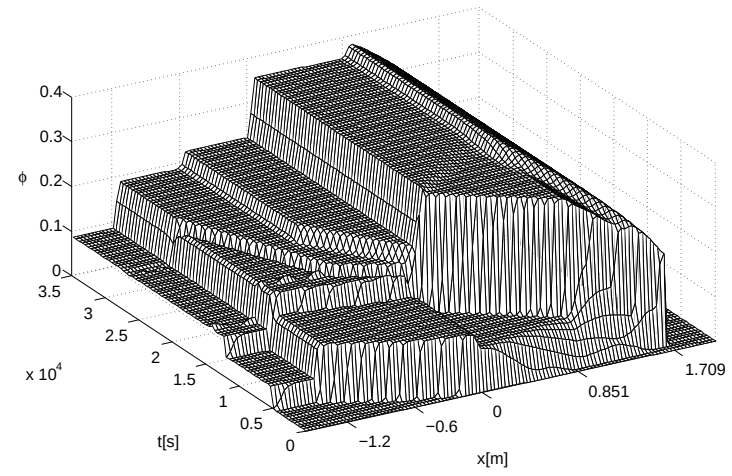

FIGURE 4. Example 1: (a) Simulated concentration ϕ_3 (species 3), (b) simulated total concentration ϕ.

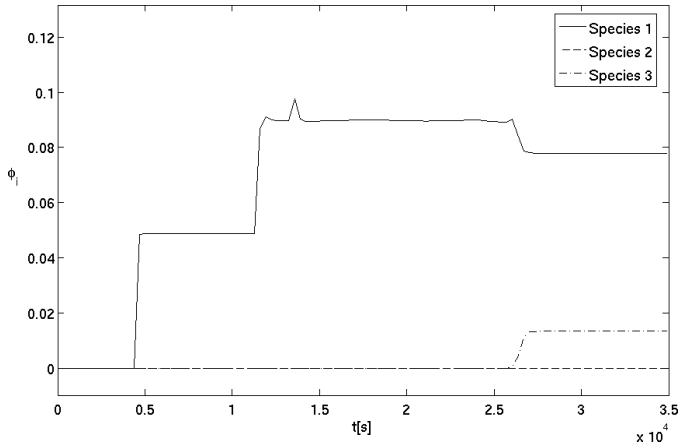

FIGURE 5. Example 1: Overflow concentrations

6.2. **Example 1.** We consider Vessel 1 with the function

$$S(x) = \begin{cases} 0.01815\,\mathrm{m}^2 & \text{for } x \le -1.200\,\mathrm{m}, \\ 0.0287\,\mathrm{m}^2 & \text{for } -1.200\,\mathrm{m} < x \le 0.915\,\mathrm{m}, \\ S_1(x) & \text{for } 0.915\,\mathrm{m} < x \le 1.709\,\mathrm{m}, \\ 8.17 \times 10^{-3}\,\mathrm{m}^2 & \text{for } x > 1.709\,\mathrm{m}, \end{cases}$$

where the conical segment is described by

$$S_1(x) := 0.7854(0.191\,\mathrm{m} - 0.1121(x - 0.915\,\mathrm{m}))^2.$$

The solids are supposed to be spheres made of of polystyrene (species 1), glass (species 2) and ballotini (species 3). We here obtain $n = 4.66$, and utilize (6.1) with $\phi_\mathrm{q} = 0.63$ and $\phi_\mathrm{max} = 0.68$. In light of the low particle Reynolds numbers, we employ the first alternative in (3.8).

Since different densities are involved here, the equations are possibly unstable for certain concentration vectors Φ. However, we evaluated the instability criterion for the numerical solution obtained here, with the result that the solution completely sojourns in the stability region. In other words, instability phenomena do not occur here.

Figures 3 (a) and (b) and Figure 4 (a) show the simulated concentrations ϕ_1, ϕ_2 and ϕ_3 until a steady state is attained. We observe in Figures 5 and 6 that the overflow, upper sink, and lower sink streams are mainly composed by species 1, 3, and 2, respectively. Figure 4 (b) shows the total volume fraction of solids for this example.

6.3. **Example 2.** We here adopt experimental data by Chen et al. (2002a, Figure 3) for the steady-state separation of a bidisperse suspension in a liquid fluidized bed classifier. Vessel 2 corresponds to

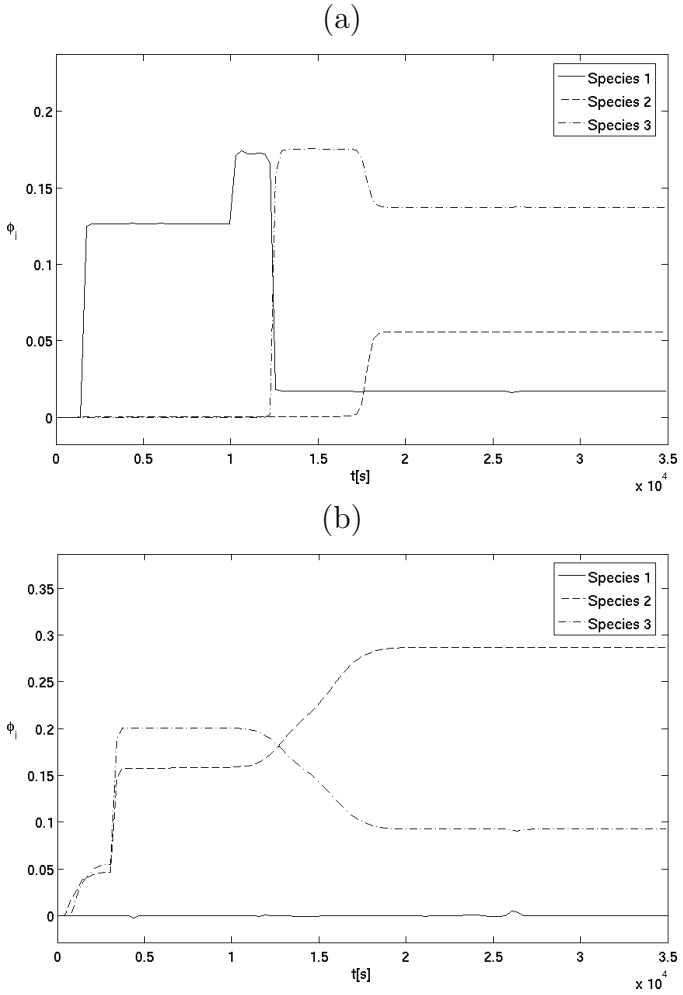

FIGURE 6. Example 1: (a) Upper, (b) lower sink concentrations.

equipment "T-2" of Chen et al. (2002a), and is described by

$$S(x) = \begin{cases} 4.54 \times 10^{-3}\,\mathrm{m}^2 & \text{for } x \le -0.165\,\mathrm{m}, \\ 0.0287\,\mathrm{m}^2 & \text{for } -0.165\,\mathrm{m} < x \le 0.915\,\mathrm{m}, \\ S_2(x) & \text{for } 0.915\,\mathrm{m} < x \le 1.709\,\mathrm{m}, \\ 2.04 \times 10^{-3}\,\mathrm{m}^2 & \text{for } x > 1.709\,\mathrm{m}, \end{cases}$$

including a conical segment defined by

$$S_2(x) := 0.7854(0.191\,\mathrm{m} - 0.1763(x - 0.915\,\mathrm{m}))^2.$$

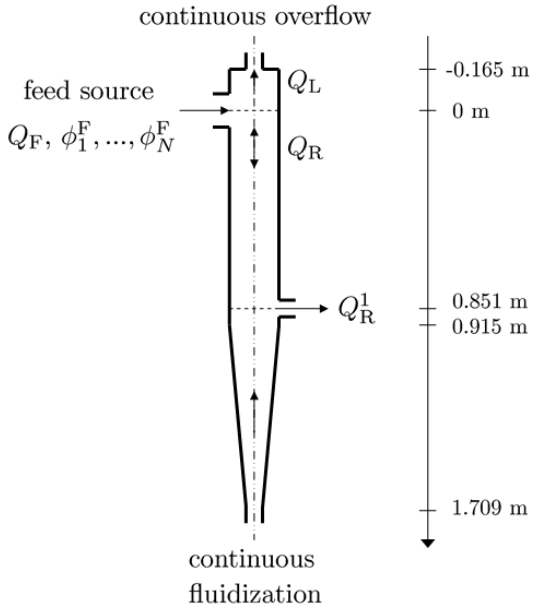

FIGURE 7. Vessel 2 with varying interior area and one sink.

The solids parameters correspond to glass beads of two sizes. For this suspension, we obtain $n = 2.91$ and use (6.1) with $\phi_{\mathrm{q}} = 0.63$ and $\phi_{\max} = 0.68$, and use the second alternative of (3.8) with $\beta = 0.65$.

Figure 8 shows the simulated concentrations ϕ_1 and ϕ_2 until a steady state state is attained. Figure 9 presents the total concentration of solids. We observe in Figure 10 that at steady state, species 1 and 2 leave the vessel by the sink stream and overflow, with an increase of the concentration of species 1 and a decrease of that of species 2 with respect to the feed concentration, whereas in the overflow, concentrations of both species are smaller in relation to feed. Figure 11 indicates that the model fits reasonably well the experimental data.

6.4. **Example 3.** Chen et al. (2002a) also study the steady-state separation of a suspension with a continuous particle size distribution fitted by the Rosin-Rammler equation, showing results for six representative species. We here apply our model to a suspension composed of $N = 6$

(a)

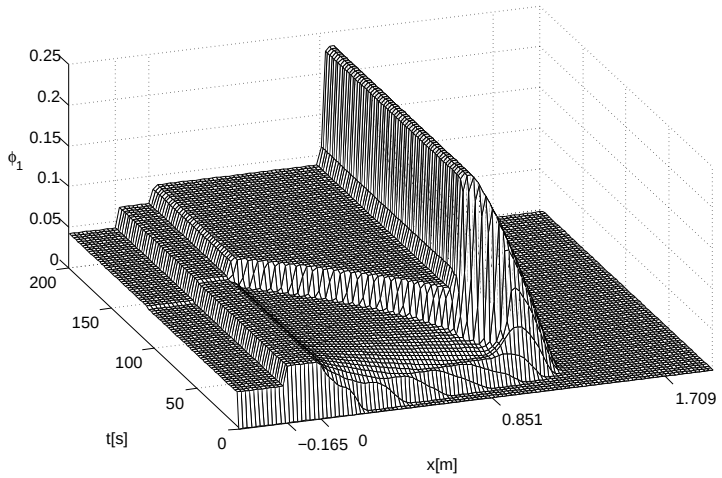

(b)

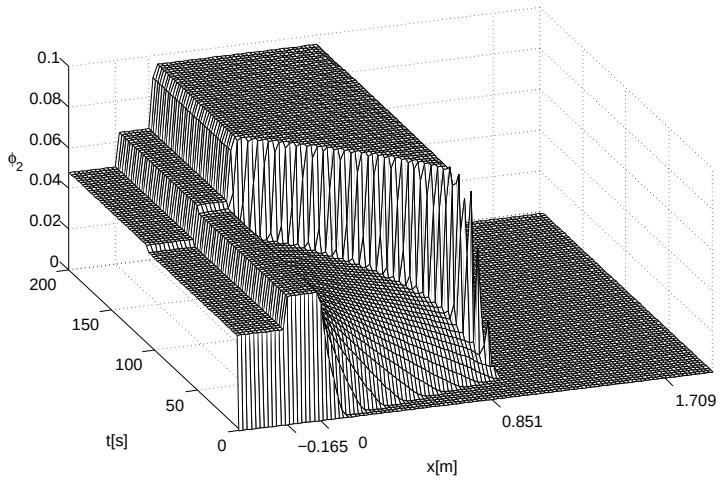

FIGURE 8. Example 2: Simulated concentrations (a) ϕ_1 (large particles), (b) ϕ_2 (small particles).

species, adopting the experimental data by Chen et al. (2002a). Vessel 3 corresponds to their equipment "C-0", and is described by

$$S(x) = \begin{cases} 4.54 \times 10^{-3}\,\mathrm{m}^2 & \text{for } x \le -0.165\,\mathrm{m}, \\ 0.0670\,\mathrm{m}^2 & \text{for } -0.165\,\mathrm{m} < x \le 0.127\,\mathrm{m}, \\ S_3(x) & \text{for } 0.127\,\mathrm{m} < x \le 0.229\,\mathrm{m}, \\ 0.0287\,\mathrm{m}^2 & \text{for } 0.229\,\mathrm{m} < x \le 0.915\,\mathrm{m}, \\ S_4(x) & \text{for } 0.915\,\mathrm{m} < x \le 1.372\,\mathrm{m}, \\ 2.04 \times 10^{-3}\,\mathrm{m}^2 & \text{for } x > 1.372\,\mathrm{m}, \end{cases}$$

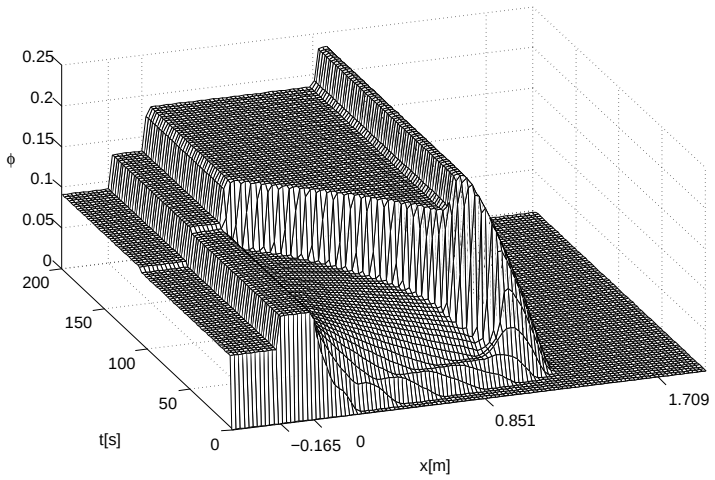

FIGURE 9. Example 2: Simulated total concentration ϕ.

including conical segments defined by

$$S_3(x) := 0.7854(0.292\,\mathrm{m} - 0.9902(x - 0.127\,\mathrm{m}))^2,$$
$$S_4(x) := 0.7854(0.191\,\mathrm{m} - 0.3063(x - 0.915\,\mathrm{m}))^2.$$

The solids parameters correspond to glass beads of six different sizes. We here obtain $n = 2.74$, and use (6.1) with $\phi_\mathrm{q} = 0.95$ and $\phi_\mathrm{max} = 1.0$, along with the second alternative of (3.8) with $\beta = 0.3$. Figures 13 (a) and (b) and Figure 15 (a) shows the simulated concentrations ϕ_1, ϕ_3 and ϕ_6 until a steady state is attained. In Figure 15 (b) we show the total concentration ϕ for this simulation. We observe in Figure 15 that at steady state, all species leave the vessel by the overflow, whereas only species 1, 2, 3 and 4 leave the vessel by the sink stream.

Figure 16 displays the relative volume fraction $C_i := \phi_i/\phi$, $i = 1, \ldots, N$, at steady state, i.e., after a simulated time of $t = 500\,\mathrm{s}$, within the unit. Thus, we can compare numerical results with measurements displayed in Figure 5 of Chen et al. (2002a). Our Figure 16 shows that for this example our model agrees well with the experimental data.

7. Conclusions

The discontinuous-flux CT model for the continuous solid-liquid separation of suspensions has been extended to a generalized clarifier-thickener model (GCT), in which an arbitrary number of discharge streams (or products) is described by singular sink terms. This feature

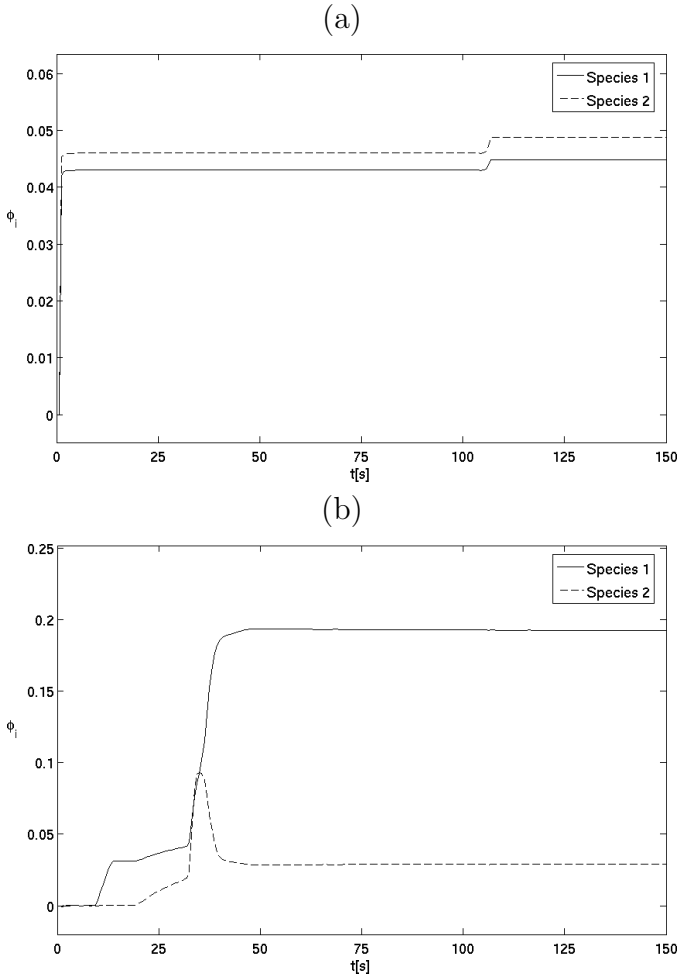

FIGURE 10. Example 2: (a) Overflow, (b) sink concentrations.

allows us to describe the continuous extraction of products of different composition. A GCT can be operated either in the CT mode or in the FC mode, depending on whether the feed bulk flow is split into diverging bulk flows or not. Such a unit can be employed for continuous solid-liquid separation or classification of suspensions. To this end, the GCT setup is combined with a kinematic model of sedimentation of polydisperse suspensions. The governing equation of the resulting model is a strongly coupled system of nonlinear conservation laws that has a discontinuous flux and a non-conservative transport term describing the sinks. A numerical algorithm for the solution of this system has been presented, along with three numerical examples. The model provides a complete description of the GCT unit including all critical

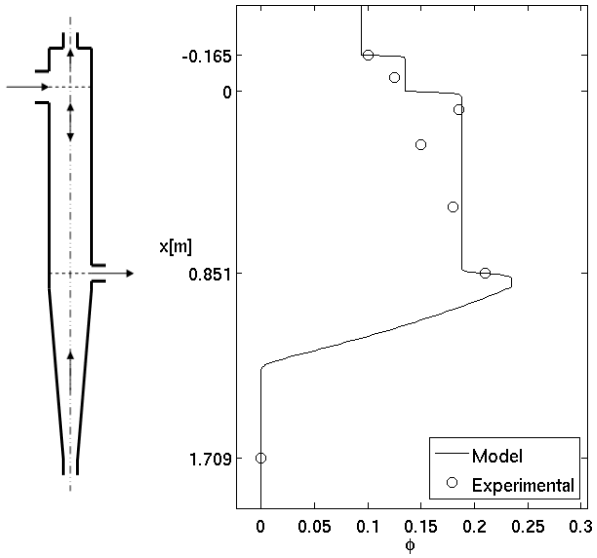

FIGURE 11. Example 2: Comparison of total concentration ϕ in steady state predicted by the model with experimental data extracted from Chen et al. (2002a).

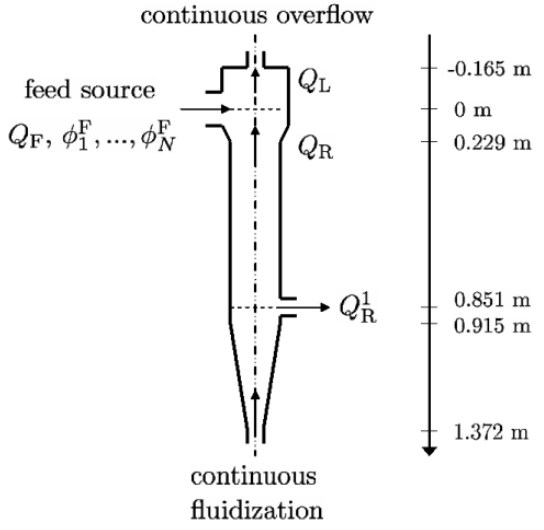

FIGURE 12. Vessel 3 with varying interior area and one sink.

design parameters, and predicts the composition of the overflow, underflow and discharge streams as well as the spatio-temporal evolution of the composition inside the unit.

(a)

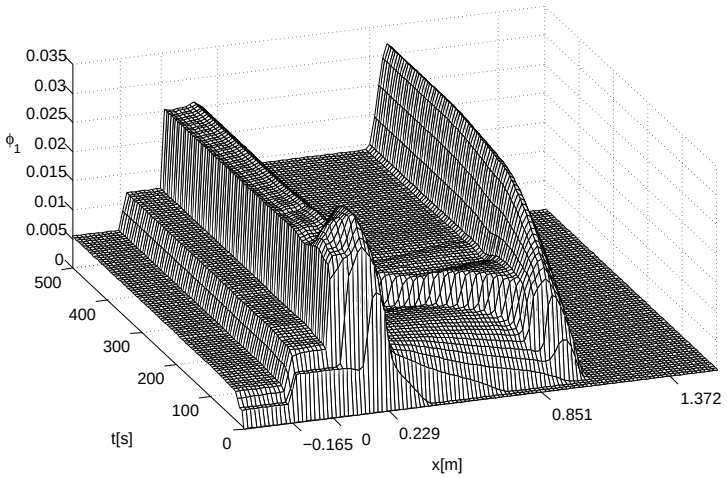

(b)

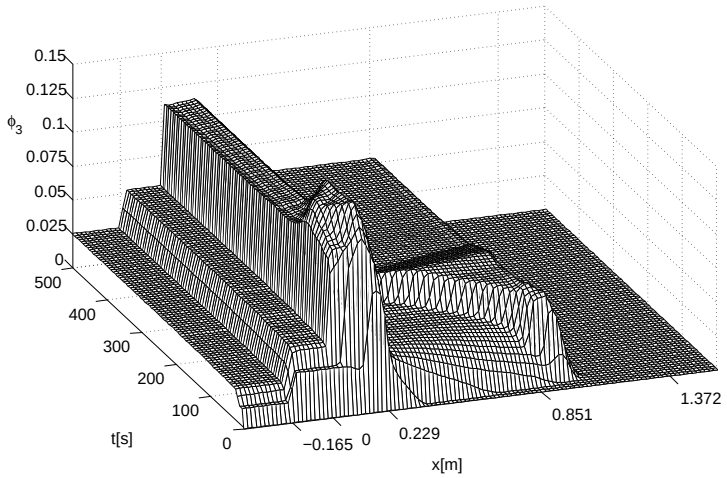

FIGURE 13. Example 3: Simulated concentrations (a) ϕ_1 (largest species), (b) ϕ_3 (medium species).

Clearly, the model presented herein is subject to limitations that already appear in the assumptions stated in Sections 2–4. Obviously, the model applies only to units that are (at least approximately) one-dimensional, and where lateral concentration or velocity gradients are

(a)

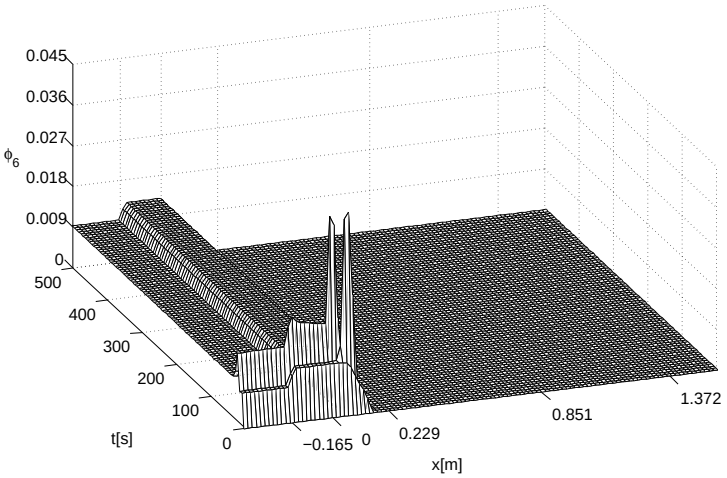

(b)

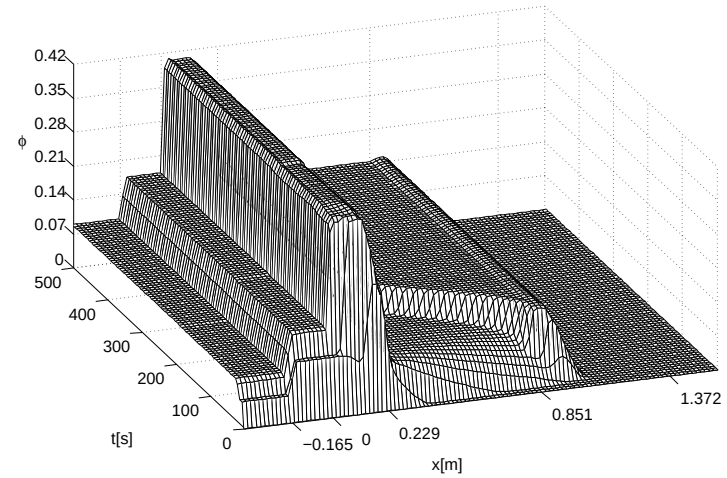

FIGURE 14. Example 3: (a) Simulated concentration ϕ_6 (smallest species), (b) simulated total concentration ϕ.

negligible. This means, for example, that particles should be reasonably small, so that wall effects are unimportant, and that inclined settlers are at present excluded. It also presumed that the model parameters for the MLB framework are known, for example from batch settling experiment. The MLB framework actually presumes that particles are

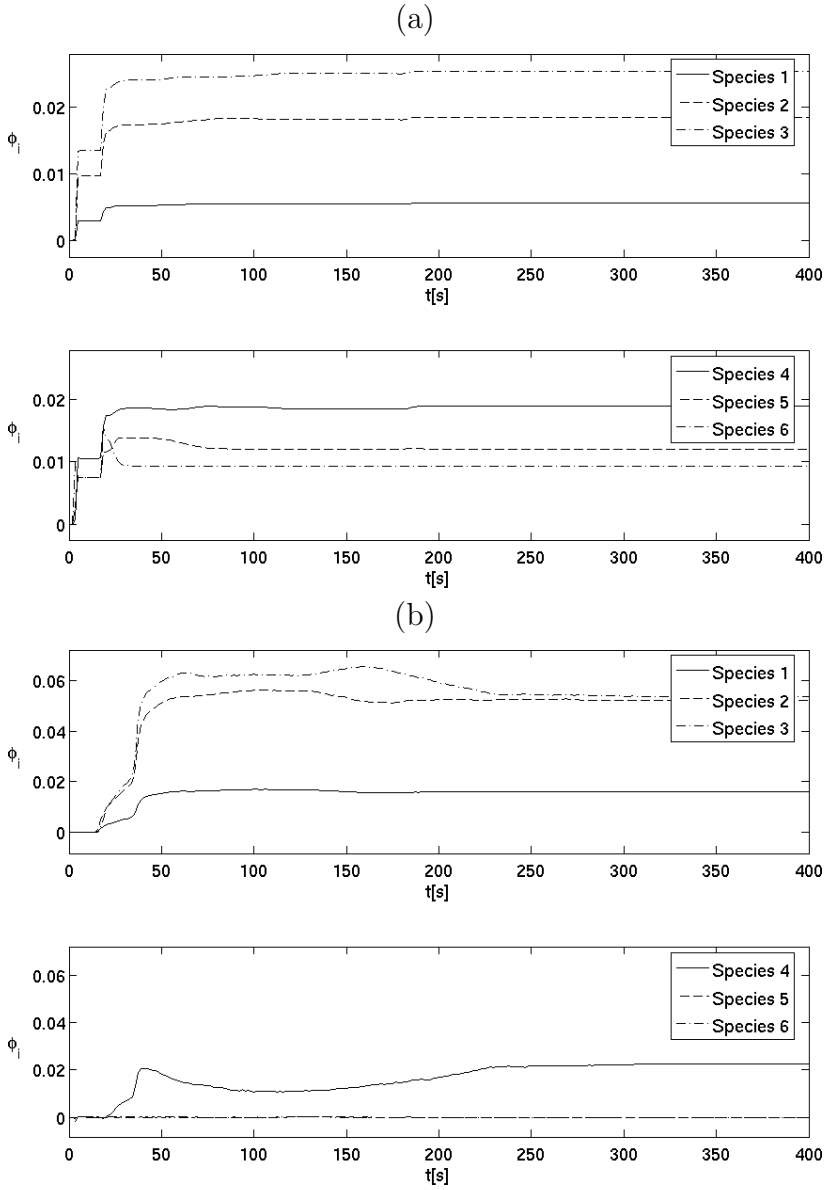

FIGURE 15. Example 3: (a) Overflow concentrations, (b) sink concentrations.

small rigid spheres. While sphericality can be considered as a useful approximation for particles of slightly more general geometry, the rigidity of particles is essential. For example, soft particles, such as flocs, form compressible sediments with curved iso-concentration lines, which cannot be captured by a purely kinematic model; rather, dynamic effects

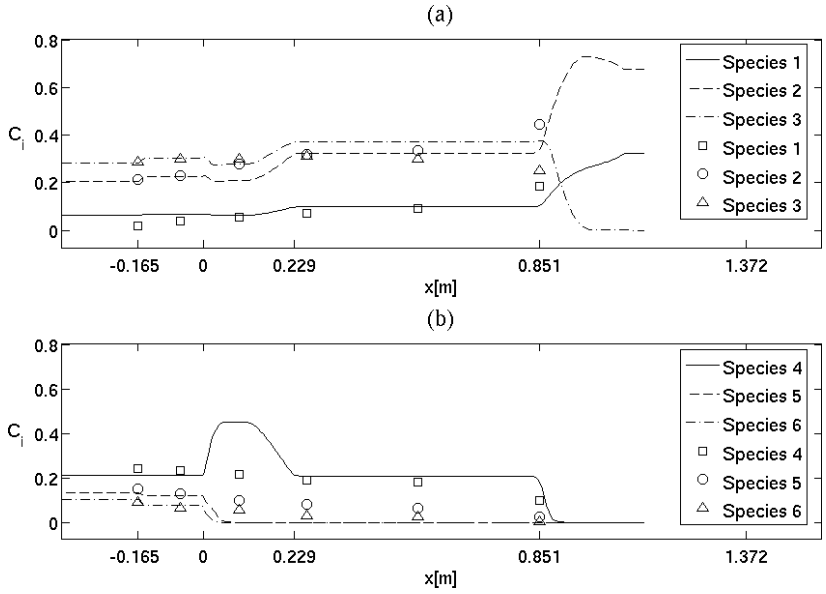

FIGURE 16. Example 3: Comparison of simulated normalized solids volume fractions $C_i = \phi_i/\phi$ with experimental data by Chen et al. (2002a, Figure 5).

such as effective solids stress have to be taken into account. This can be achieved by a degenerate hyperbolic-parabolic system of equations, which is slightly more involved than (4.6), see Berres et al. (2003).

ACKNOWLEDGMENTS

RB is supported by FONDECYT projects 1050728 and 7060104, and FONDAP in Applied Mathematics. AG acknowledges support by MECESUP project UCO 0406. The research of KHK is supported by an Outstanding Young Investigators Award (OYIA) from the Research Council of Norway. Part of this research was done while AG visited CMA at the University of Oslo, and he is grateful to MECESUP and OYIA for financial support. JDT acknowledges support by FONDECYT project 7060104 while visiting the University of Concepción.

REFERENCES

Batchelor, G.K., & Janse van Rensburg, R.W. (1986). Structure formation in bidisperse sedimentation. *Journal of Fluid Mechanics*, *166*, 379–407.

Berres, S., Bürger, R., Karlsen, K.H., & Tory, E.M. (2003). Strongly degenerate parabolic-hyperbolic systems modeling polydisperse

sedimentation with compression. *SIAM Journal on Applied Mathematics*, *64*, 41–80.

Berres, S., Bürger, R., & Karlsen, K.H. (2004). Central schemes and systems of conservation laws with discontinuous coefficients modeling gravity separation of polydisperse suspensions. *Journal of Computational and Applied Mathematics*, *164-165*, 53–80.

Biesheuvel, P.M., Verweij, H., & Breedveld, V. (2001). Evaluation of instability criterion for bidisperse sedimentation. *AIChE Journal*, *47*, 45–52.

Bürger, R., Concha, F., Fjelde, K.-K., & Karlsen, K.H. (2000). Numerical simulation of the settling of polydisperse suspensions of spheres. *Powder Technology*, *113*, 30–54.

Bürger, R., Concha, F., Karlsen, K.H., & Narváez, A. (2006a). Numerical simulation of clarifier-thickener units treating ideal suspensions with a flux density function having two inflection points. *Mathematical and Computer Modelling*, *44*, 255–275.

Bürger, R., García, A., Karlsen, K.H., & Towers, J.D. (2006b). On an extended clarifier-thickener model with singular source and sink terms. *European Journal of Applied Mathematics*, *17*, 257–292.

Bürger, R., Karlsen, K.H., Risebro, N.H., & Towers, J.D. (2004). Well-posedness in BV_t and convergence of a difference scheme for continuous sedimentation in ideal clarifier-thickener units. *Numerische Mathematik*, *97*, 25–65.

Bürger, R., Karlsen, K.H., Tory, E.M., & Wendland, W.L. (2002). Model equations and instability regions for the sedimentation of polydisperse suspensions of spheres. *ZAMM Zeitschrift für Angewandte Mathematik und Mechanik*, *82*, 699–722.

Bürger, R., Karlsen, K.H., & Towers, J.D. (2005). A model of continuous sedimentation of flocculated suspensions in clarifier-thickener units. *SIAM Journal on Applied Mathematics*, *65*, 882–940.

Chen, A., Grace, J.R., Epstein, N., & Lim, C.J. (2002a). Steady state dispersion of mono-size, binary and multi-size particles in a liquid fluidized bed classifier. *Chemical Engineering Science*, *57*, 991–1002.

Chen, A., Grace, J.R., Epstein, N., & Lim, C.J. (2002b). Unsteady state hydrodynamic model and dynamic behaviour of a liquid fluidized-bed classifier. *Chemical Engineering Science*, *57*, 1003–1010.

Crowe, C., Sommerfeld, M., & Tsuji, Y. (1998). Multiphase Flows with Droplets and Particles. CRC Press, Boca Raton, FL, USA.

Deen, N.G., Van Sint Annaland, M., Van der Hoef, M.A., & Kuipers, J.A.M. (2007). Review of discrete particle modelling of fluidized beds. *Chemical Engineering Science*, *62*, 28–44.

Diehl, S. (2006). Operating charts for continuous sedimentation III: Control of step input. *Journal of Engineering Mathematics*, *54*, 225–259.

Enwald, H., Peirano, E., & Almstedt, A.E. (1996). Eulerian two-phase flow theory applied to fluidization. *International Journal of Multiphase Flow*, *22* (Suppl.), 21–66.

Fried, E., & Roy, B.C. (2003). Gravity-induced segregation of cohesionless granular mixtures. In: K. Hutter, N. Kirchner (eds.), Dynamic Response of Granular and Porous Materials Under Large and Catastrophic Deformations, Springer-Verlag, Berlin, 393–421.

Gera, D., Gautam, M., Tsuji, Y., Kawaguchi, T., & Tanaka, T. (1998). Computer simulation of bubbles in large-particle fluidized beds. *Powder Technology 98*, 38–47.

Gibilaro, L.G. (2001). Fluidization-dynamics, Butterworth-Heinmann, Jordan Hill, UK.

Gidaspow, D. (1994). Multiphase Flow and Fluidization, Academic Press, San Diego, CA, USA.

Glowinski, R., Pan, T.W., Hesla, T.I., Joseph, D.D., & Périaux, J. (2001). A fictitious domain approach to the direct numerical simulation of incompressible viscous flow past moving rigid bodies: application to particulate flow. *Journal of Computational Physics*, *169*, 363–426.

Greenspan, H.P., & Ungarish, M. (1982). On hindered settling of particles of different sizes. *International Journal of Multiphase Flow*, *8*, 587–604.

Ha, Z., & Liu, S. (2002). Settling velocities of polydisperse concentrated suspensions. *Canadian Journal of Chemical Engineering*, *80*, 783–790.

Jackson, R. (2000) The Dynamics of Fluidized Particles, Cambridge University Press, Cambridge, UK.

Kawaguchi, T., Tanaka, T., & Tsuji, Y. (1998). Numerical simulation of two-dimensional fluidized beds using the discrete element method (comparison between the two- and three-dimensional models). *Powder Technology*, *96*, 129–138.

Kawaguchi, T., Sakamoto, M., Tanaka, T., & Tsuji, Y. (2000). Quasi-three-dimensional numerical simulation of spouted beds in cylinder. *Powder Technology*, *109*, 3–12.

Kim, B.H., & Klima, M.S. (2004). Development and application of a dynamic model for hindered-settling column separations. *Minerals Engineering*, *17*, 403–410.

Kunii, D., & Levenspiel, O. (1991). Fluidization Engineering. 2nd edition. Butterworth-Heinemann, Jordan Hill, UK.

Kurganov, A., & Tadmor, E. (2000). New high resolution central schemes for nonlinear conservation laws and convection-diffusion equations. *Journal of Computational Physics*, *160*, 241–282.

Kynch, G.J. (1952). A theory of sedimentation. *Transactions of the Faraday Society*, *48*, 166–176.

Law, D.H.-S., Masliyah, J.H., MacTaggart, R.S., & Nandakumar, K. (1987). Gravity separation of bidisperse suspensions: light and heavy particle species. *Chemical Engineering Science*, *42*, 1527–1538.

Lockett, M.J., & Bassoon, K.S. (1979). Sedimentation of binary particle mixtures. *Powder Technology*, *24*, 1–7.

Masliyah, J.H. (1979). Hindered settling in a multiple-species particle system. *Chemical Engineering Science*, *34*, 1166–1168.

Mitsutani, K., Grace, J.R., & Lim, C.J. (2005). Residence time distribution of particles in a continuous liquid-solid classifier. *Chemical Engineering Science*, *60*, 2703–2713.

Nasr-El-Din, H., Masliyah, J.H. & Nandakumar, K. (1990). Continuous gravity separation of concentrated bidisperse suspensions in a vertical column. *Chemical Engineering Science*, *45*, 849–857.

Nasr-El-Din, H., Masliyah, J.H., & Nandakumar, K. (1999). Continuous separation of suspensions containing light and heavy particle species. *Canadian Journal of Chemical Engineering*, *77*, 1003–1012.

Nasr-El-Din, H., Masliyah, J.H., Nandakumar, K., & Law, D.H.-S. (1988). Continuous gravity separation of a bidisperse suspension in a vertical column. *Chemical Engineering Science*, *43*, 3225–3234.

Nessyahu, H., & Tadmor, E. (1990). Non-oscillatory central differencing for hyperbolic conservation laws. *Journal of Computational Physics*, *87*, 408–463.

Nguyentranlam, G., & Galvin, K.P. (2001). Particle classification in the reflux classifier. *Minerals Engineering*, *14*, 1081–1091.

Pan, T.W., Joseph, D.D., Bai, R., Glowinski, R., & Sarin, V. (2002). Fluidization of 1204 spheres: simulation and experiment. *Journal of Fluid Mechanics*, *451*, 169–191.

Qian, S., Bürger, R., & Bau, H.H. (2005). Analysis of sedimentation biodetectors. *Chemical Engineering Science*, *60*, 2585–2598.

Richardson, J.F., & Zaki, W.N. (1954). Sedimentation and fluidization: Part I. *Transactions of the Institution of Chemical Engineers (London)*, *32*, 35–53.

Spannenberg, A., Galvin, K., Raven, J., & Scarboro, M. (1996). Continuous differential sedimentation of a binary suspension. *Chemical Engineering in Australia*, *21*, 7–11.

Tsuji, Y., Kawaguchi, T., & Tanaka, T. (1993). Discrete particle simulation of two-dimensional fluidized bed. *Powder Technology*, *77*, 79–87.

Tsuji, Y., Tanaka, T., & Yonemura, S. (1998). Cluster patterns in circulating fluidized beds predicted by numerical simulation (discrete particle model versus two-fluid model). *Powder Technology*, *95*, 254–264.

Weiland, R.H., Fessas, Y.P., & Ramarao, B.V. (1984). On instabilities arising during sedimentation of two-component mixtures of solids. *Journal of Fluid Mechanics*, *142*, 383–389.

Yamamoto, Y., Potthoff, M., Tanaka, T., Kajishama, T., & Tsuji, Y. (2001). Large-eddy simulation of turbulent gas-particle flow in a vertical channel: effect of considering inter-particle collisions. *Journal of Fluid Mechanics*, *442*, 303–334.

Young, M.L., & Klima, M.S. (2000). Evaluation of a hindered-settling column for size/density separations. *Minerals & Metallurgical Processing*, *17*, 194–197.

Zeidan, A., Rohani, S., & Bassi, A. (2004). Dynamic and steady-state sedimentation of polydisperse suspension and prediction of outlets particle-size distribution. *Chemical Engineering Science*, *59*, 2619–2632.

Zeidan, A., Rohani, S., Bassi, A., & Whiting, P. (2003). Review and comparison of solids settling velocity models. *Reviews in Chemical Engineering*, *19*, 473–530.